

HIGH ORDER ASYMPTOTIC PRESERVING SCHEME FOR DIFFUSIVE SCALED LINEAR KINETIC EQUATIONS WITH GENERAL INITIAL CONDITIONS

MEGALA ANANDAN¹, BENJAMIN BOUTIN^{2,*} AND NICOLAS CROUSEILLES³

Abstract. Diffusive scaled linear kinetic equations appear in various applications, and they contain a small parameter ϵ that forces a severe time step restriction for standard explicit schemes. Asymptotic preserving (AP) schemes are those schemes that attain asymptotic consistency and uniform stability for all values of ϵ , with the time step restriction being independent of ϵ . In this work, we develop high order AP scheme for such diffusive scaled kinetic equations with both well-prepared and non-well-prepared initial conditions by employing IMEX-RK time integrators such as CK-ARS and A types. This framework is also extended to a different collision model involving advection-diffusion asymptotics, and the AP property is proved formally. A further extension of our framework to inflow boundaries has been made, and the AP property is verified. The temporal and spatial orders of accuracy of our framework are numerically validated in different regimes of ϵ , for all the models. The qualitative results for diffusion asymptotics, and equilibrium and non-equilibrium inflow boundaries are also presented.

Mathematics Subject Classification. 82C40, 85A25, 65M06, 65L04, 65L06.

Received August 29, 2023. Accepted April 13, 2024.

1. INTRODUCTION

In this work, we are concerned with the numerical approximation of linear collisional kinetic transport equations in a diffusive scaling. Such models are widely used in applications such as rarefied gas dynamics, neutron transport, and radiative transfer. Due to the presence of a small parameter ϵ (which is the normalized mean free path of the particles), standard explicit schemes suffer from a severe restriction on the numerical parameters so that they experience extremely high computational cost as $\epsilon \rightarrow 0$. In the last decades, the so-called Asymptotic-Preserving (AP) schemes have been proposed to make the numerical passage between the micro and macro scale [19, 23, 24] possible. Indeed, these AP schemes are uniformly stable (*i.e.*, the numerical parameters can be chosen independent of ϵ and degenerate when $\epsilon \rightarrow 0$ to a scheme which is consistent with the asymptotic model). These schemes efficiently deal with multi-scale phenomena and are a viable alternative to domain decomposition approaches.

Keywords and phrases. Collisional kinetic equation, diffusive scaling, high order Runge–Kutta schemes, asymptotic preserving property.

¹ Indian Institute of Science, C.V. Raman Road, Bangalore 560012, India.

² Univ Rennes, CNRS, IRMAR UMR 6625, 35000 Rennes, France.

³ Univ Rennes, CNRS, IRMAR UMR 6625 & Centre Inria de l'Université de Rennes (MINGuS) & ENS Rennes, Rennes, France.

*Corresponding author: benjamin.boutin@univ-rennes.fr

In this work, we are concerned with high order in time AP scheme for collisional kinetic equations in the diffusive scaling, possibly involving boundary conditions. Several works can be found in the literature on this topic using splitting method, odd-even or micro-macro decompositions (see [4, 13, 18, 19, 22–25, 25–28, 30, 31, 34]). Our work is based on a micro-macro decomposition as introduced in [30] where the unknown f of the stiff kinetic equation is split into an equilibrium part ρ and a remainder g . A micro-macro model (equivalent to the original kinetic one) satisfied by ρ and g can be derived. This micro-macro strategy turns out to be the starting point of several numerical approximation in phase space (using staggered grid [30], particles method [7, 8, 13], Discontinuous Galerkin method [17, 33–35] or low rank approximation [14, 15]). Regarding the time discretization, a suitable first order semi-implicit time discretization of the micro-macro model has been initially proposed in [30] for which the AP property is ensured for general initial conditions. High order extensions are usually based on IMEX Runge–Kutta methods [2, 3, 5, 6, 12, 32] which turns out to be a useful framework to derive high order AP schemes for stiff kinetic equations under a fluid scaling [1, 9–11]. but also under a diffusive scaling [16, 17]; in these works however, even if the proposed numerical schemes enjoy the AP property and are high order, the asymptotic diffusion equation is solved explicitly, leading to a stringent parabolic CFL condition for small ϵ . This drawback is overcome using a suitable modification to the semi-implicit time discretization of [30] which results in a first order implicit scheme for the asymptotic diffusion equation that is devoid of the parabolic CFL condition (see [7, 8, 28]). High order versions have been derived and analyzed in [4, 33–35], leading to a numerical scheme which is asymptotically free from the usual restrictive parabolic condition.

In this work, a family of high order IMEX numerical schemes is proposed for linear collisional kinetic equations in the diffusive scaling. According to the collision operator, the asymptotic model can be a pure diffusion equation or an advection-diffusion equation as in [17]. The numerical schemes presented in this work are high order, uniformly stable with respect to ϵ and degenerate when $\epsilon \rightarrow 0$ to a high order implicit scheme for the pure asymptotic diffusion equation or to a high order IMEX scheme of the asymptotic advection-diffusion equation. From the first order semi-implicit AP numerical scheme [8], the family of high order schemes proposed in this work is obtained using globally stiffly accurate high order IMEX Runge–Kutta methods, namely type A and type CK [10, 17]. In particular, we discuss the AP property according to the considered class (type A or CK) and according to the initial condition (well-prepared or not). For the two cases (diffusion and advection-diffusion), the AP property is proved with general initial condition (referred as strong AP property in the literature).

Our work bears similarities with the series of works [33–35] in which high order AP schemes are derived and analyzed for linear collisional kinetic equations in the diffusive scaling. However, there are some differences. Indeed, in [34, 35], an artificial weighted diffusion is added and subtracted to get an implicit scheme for the parabolic term, in the spirit of [4]; but, as mentioned in [33], this weighted diffusion term may depend on ϵ and/or the numerical parameters, and has to be chosen according to the considered problem which can affect the performance of the numerical simulations. As in [33], the numerical schemes proposed in this work directly solve the micro-macro system. Another difference lies in the choice of time integrator (type A, in particular) that allows the scheme to be asymptotic preserving when the initial data is not well-prepared, without requiring the reduction of initial time steps (the numerical methods proposed in [33, 35] require the time step to be Δt^p for p th order accurate scheme in the initial few steps). Further, we consider here advection-diffusion problems and problems involving incoming boundary conditions; our family of high order scheme can be easily extended to the half moment micro-macro decomposition introduced in [29] to naturally incorporate incoming boundary conditions, even when non well prepared boundary conditions are considered.

Lastly, we address the space discretization in order to get a fully high order solver of the stiff kinetic equation. Let us mention Discontinuous Galerkin methods developed in [17, 33–35] for similar purposes. Here we focus on high order classical finite difference methods for the space approximation which only involve a discrete diffusion term to invert. Staggered or non-staggered strategies are discussed.

The paper is organized as follows. First in Section 2, the kinetic and asymptotic diffusion models are introduced. Then in Section 3, high order time integrators (using globally stiffly accurate IMEX Runge–Kutta temporal discretization) are proposed, and their AP property in the diffusive limit is addressed in Section 4. Section 5 is devoted to the space approximation. In Section 6, we discuss some extensions to other collision

operators and to half moments. In Section 7, numerical results are presented, illustrating high order accuracy and the main properties of the schemes.

2. KINETIC EQUATION, DIFFUSION LIMIT AND MICRO-MACRO DECOMPOSITION

In this section, we introduce the kinetic model in diffusive scaling, and recall the asymptotic limit. Then, the micro-macro decomposition is performed to derive the micro-macro model which serves as a basis for numerical developments.

2.1. Linear kinetic equation with diffusive scaling

Let $\Omega \subset \mathbb{R}^d$ be the position space and $V \subseteq \mathbb{R}^d$ be the velocity space with measure $d\mu(v)$. We consider the linear kinetic equation with diffusive scaling,

$$\partial_t f + \frac{1}{\epsilon} v \cdot \nabla_x f = \frac{1}{\epsilon^2} Lf, \quad (t, x, v) \in \mathbb{R}^+ \times \Omega \times V \quad (2.1)$$

where $f(t, x, v) \in \mathbb{R}$ is the distribution function (depending on time $t \in \mathbb{R}^+$, space $x \in \Omega \subset \mathbb{R}^d$ and velocity $v \in V \subset \mathbb{R}^d$) and $\epsilon > 0$ measures the dimensionless mean free path of particles or the inverse of relaxation time. We consider the initial condition,

$$f(0, x, v) = f^{\text{init}}(x, v), \quad (x, v) \in \Omega \times V \quad (2.2)$$

and boundary conditions are imposed in space. In this work, we will consider periodic boundary conditions or inflow boundary conditions. The linear collision operator L in equation (2.1) acts only on the velocity dependence of f , and it relaxes the particles to an equilibrium $M(v)$ which is positive and even. We denote for all velocity dependent distribution functions h ,

$$\langle h \rangle_V = \frac{\int_V h(v) d\mu}{\int_V M(v) d\mu}. \quad (2.3)$$

In particular, we obtain $\langle M \rangle_V = 1$ and $\langle vM \rangle_V = 0$. Further, the operator L is non-positive and self-adjoint in $L^2(V, M^{-1} d\mu)$, with the following null space and range:

$$\mathcal{N}(L) = \{f : f \in \text{Span}(M)\}, \quad \mathcal{R}(L) = (\mathcal{N}(L))^\perp = \{f : \langle f \rangle_V = 0\}. \quad (2.4)$$

Therefore, L is invertible on $\mathcal{R}(L)$ and we denote its pseudo-inverse by L^{-1} .

2.2. Diffusion limit

In the limit $\epsilon \rightarrow 0$, it is seen from equation (2.1) that $f \rightarrow f_0$ where f_0 belongs to $\mathcal{N}(L)$. Thus, $f_0 = \rho(t, x)M$ where f_0 solves $Lf_0 = 0$ and where the limiting density ρ is the solution of the asymptotic diffusion equation. To derive the diffusion equation, a Chapman–Enskog expansion has to be performed to get $f = f_0 + \epsilon L^{-1}(vM) \cdot \nabla_x \rho + \mathcal{O}(\epsilon^2)$. Integrating with respect to the velocity variable enables to get the diffusion limit

$$\partial_t \rho - \nabla_x \cdot (\kappa \nabla_x \rho) = 0 \quad \text{with} \quad \kappa = -\langle v \otimes L^{-1}(vM) \rangle_V > 0. \quad (2.5)$$

2.3. Micro-macro decomposition

In this part, we derive a micro-macro model which is equivalent to (2.1), and this is the model that will be discretized in the next sections. First, we consider the standard micro-macro decomposition of the unknown f [28, 30],

$$f = \rho M + g, \quad \text{with} \quad \rho(t, x) = \langle f \rangle_V \quad \text{and} \quad \langle g \rangle_V = 0. \quad (2.6)$$

We introduce the orthogonal projector Π in $L^2(V, M^{-1} d\mu)$ onto $\mathcal{N}(L)$: $\Pi h = \langle h \rangle_V M$, which will be useful to derive the micro-macro model. Substituting equation (2.6) into equation (2.1) and applying successively Π and $(I - \Pi)$ enables to get the micro-macro model satisfied by (ρ, g)

$$\partial_t \rho + \frac{1}{\epsilon} \nabla_x \cdot \langle v g \rangle_V = 0, \tag{2.7}$$

$$\partial_t g + \frac{1}{\epsilon} (I - \Pi)(v \cdot \nabla_x g) + \frac{1}{\epsilon} v M \cdot \nabla_x \rho = \frac{1}{\epsilon^2} L g. \tag{2.8}$$

Initial conditions for macro and micro equations become

$$\rho(0, x) = \rho^{\text{init}}(x) = \langle f^{\text{init}}(x, \cdot) \rangle_V, \tag{2.9}$$

$$g(0, x, v) = g^{\text{init}}(x, v) = f^{\text{init}}(x, v) - \rho^{\text{init}}(x) M(v), \tag{2.10}$$

whereas the boundary conditions for ρ and g become periodic if f is periodic. From the micro part (2.8), a Chapman–Enskog expansion of g can be performed to get

$$g = -\epsilon (\epsilon^2 \partial_t - L)^{-1} ((I - \Pi)(v \cdot \nabla_x g) + v M \cdot \nabla_x \rho) = \epsilon L^{-1} (v M) \cdot \nabla_x \rho + \mathcal{O}(\epsilon^2),$$

under some suitable smoothness assumptions. Inserting this expression in equation (2.7) leads to equation (2.5) in the limit $\epsilon \rightarrow 0$.

3. TIME INTEGRATORS

In this part, we present the family of high order time integrators for the micro-macro model (2.7) and (2.8). We will keep the phase space variables continuous to ease the reading. We first recall the first order temporal scheme which leads to the implicit treatment of the asymptotic diffusion model before introducing the high order version.

3.1. First order accurate time integrator

Given ρ^n, g^n that approximate ρ, g at time $t = n\Delta t$, we obtain the solution ρ^{n+1}, g^{n+1} from the following time integration of equations (2.7) and (2.8) respectively. We use the following first order implicit-explicit (IMEX) strategy to attain the asymptotic preserving property

$$\rho^{n+1} = \rho^n - \frac{\Delta t}{\epsilon} \nabla_x \cdot \langle v g^{n+1} \rangle_V, \tag{3.1}$$

$$g^{n+1} = g^n - \frac{\Delta t}{\epsilon} (I - \Pi)(v \cdot \nabla_x g^n) - \frac{\Delta t}{\epsilon} v M \cdot \nabla_x \rho^{n+1} + \frac{\Delta t}{\epsilon^2} L g^{n+1}. \tag{3.2}$$

The implicit treatment of density gradient in micro equation (3.2) and fully implicit treatment of the macro equation enables us to get an implicit scheme for diffusion equation in the limit $\epsilon \rightarrow 0$.

Although the macro equation is treated in a fully implicit manner, ρ^{n+1} and g^{n+1} can be updated using equations (3.1) and (3.2) in an explicit manner. From equation (3.2), we get

$$g^{n+1} = (\epsilon^2 I - \Delta t L)^{-1} (\epsilon^2 g^n - \epsilon \Delta t (I - \Pi)(v \cdot \nabla_x g^n) - \epsilon \Delta t v M \cdot \nabla_x \rho^{n+1}). \tag{3.3}$$

Inserting this in equation (3.1), we obtain the following implicit scheme for the macro unknown

$$\rho^{n+1} = \rho^n - \Delta t \nabla_x \cdot \left\langle v (\epsilon^2 I - \Delta t L)^{-1} (\epsilon g^n - \Delta t (I - \Pi)(v \cdot \nabla_x g^n) - \Delta t v M \cdot \nabla_x \rho^{n+1}) \right\rangle_V,$$

or, expressing ρ^{n+1} as quantities at iteration n

$$\rho^{n+1} = (I - \Delta t^2 \nabla_x \cdot (\mathcal{D}_{\epsilon, \Delta t} \nabla_x))^{-1} \left(\rho^n - \Delta t \nabla_x \cdot \left\langle v (\epsilon^2 I - \Delta t L)^{-1} (\epsilon g^n - \Delta t (I - \Pi)(v \cdot \nabla_x g^n)) \right\rangle_V \right)$$

with $\mathcal{D}_{\epsilon, \Delta t} = \langle v \otimes (\epsilon^2 I - \Delta t L)^{-1} (vM) \rangle_V$. Thanks to this time integrator, ρ^{n+1} can be updated by inverting a diffusion type operator. Following this, g^{n+1} can be found explicitly from the knowledge of ρ^{n+1} . This first order scheme introduced in [8, 28] is the basis of the high order scheme presented below.

3.2. High order accurate time integrators

Following previous works [4, 10, 17, 35], we will consider globally stiffly accurate (GSA) IMEX Runge–Kutta (RK) schemes to construct high order time integrators for the micro-macro model equations (2.7) and (2.8). An IMEX RK scheme is represented using the double Butcher tableau [2, 6]

$$\begin{array}{c|c} \tilde{c} & \tilde{A} \\ \hline & \tilde{b}^T \end{array} \quad \begin{array}{c|c} c & A \\ \hline & b^T \end{array} \quad (3.4)$$

where $\tilde{A} = (\tilde{a}_{ij})$ and $A = (a_{ij})$ are $s \times s$ matrices which correspond to the explicit and implicit parts of the scheme (A and \tilde{A} respectively are lower triangular and strictly lower triangular matrices). The coefficients \tilde{c} and c are given by $\tilde{c}_i = \sum_{j=1}^{i-1} \tilde{a}_{ij}$, $c_i = \sum_{j=1}^i a_{ij}$, and the vectors $\tilde{b} = (\tilde{b}_j)$ and $b = (b_j)$ give quadrature weights that combine the stages. For GSA IMEX RK scheme, we have

$$c_s = \tilde{c}_s = 1 \text{ and } a_{sj} = b_j, \tilde{a}_{sj} = \tilde{b}_j, \quad \forall j \in \{1, 2, \dots, s\}. \quad (3.5)$$

An IMEX RK method is type A if the matrix A is invertible, and it is type CK if the first row of matrix A has zero entries and the square sub-matrix formed by excluding the first column and row of A is invertible. In the special case where the first column of A has zero entries, the scheme is said to be of type CK-ARS. The reader is referred to [10] for more details. In this work, we employ both type A and CK-ARS schemes.

The first order GSA IMEX RK scheme employed in equations (3.1) and (3.2) follows the type CK-ARS double Butcher tableau (known as ARS(1, 1, 1)),

$$\begin{array}{c|ccc} 0 & 0 & 0 & & 0 & 0 & 0 \\ 1 & 1 & 0 & & 1 & 0 & 1 \\ \hline & 1 & 0 & & 0 & 1 & \end{array} \quad (3.6)$$

We now use the general IMEX RK scheme from (3.4) with GSA property equation (3.5) for obtaining high order accurate time integration of macro and micro equations (2.7) and (2.8) respectively. We introduce the following notations in the presentation of our scheme.

$$\mathcal{T}h^{(k)} = (I - \Pi) \left(v \cdot \nabla_x h^{(k)} \right), \quad (3.7)$$

$$\mathcal{D}_{\epsilon, \Delta t}^{(j)} = \left\langle v \otimes (\epsilon^2 I - a_{jj} \Delta t L)^{-1} (vM) \right\rangle_V, \quad (3.8)$$

$$\mathcal{I}_{\epsilon, \Delta t}^{(j)} = (\epsilon^2 I - a_{jj} \Delta t L)^{-1}. \quad (3.9)$$

We will construct high order IMEX RK schemes following the first order guidelines (fully implicit treatment of macro equation, implicit treatment of density gradient and relaxation terms and explicit treatment of transport term in micro equation). Given ρ^n, g^n that approximate ρ, g at time $t = n\Delta t$, we obtain the internal RK stage values $\rho^{(j)}$ and $g^{(j)}$, $j = 1, \dots, s$ as

$$\rho^{(j)} = \rho^n - \sum_{k=1}^j a_{jk} \frac{\Delta t}{\epsilon} \nabla_x \cdot \left\langle v g^{(k)} \right\rangle_V, \quad (3.10)$$

$$g^{(j)} = g^n - \sum_{k=1}^{j-1} \tilde{a}_{jk} \frac{\Delta t}{\epsilon} \mathcal{T}g^{(k)} - \sum_{k=1}^j a_{jk} \frac{\Delta t}{\epsilon} vM \cdot \nabla_x \rho^{(k)} + \sum_{k=1}^j a_{jk} \frac{\Delta t}{\epsilon^2} Lg^{(k)}, \quad (3.11)$$

where, as usual, the summation $\sum_{k=1}^{j-1}$ in the explicit term is zero for $j = 1$.

Although the expressions above are implicit, the stage values $\rho^{(1)}, g^{(1)}$ can be found in an explicit manner by using the known quantities ρ^n, g^n , and the stage values $\rho^{(j)}, g^{(j)}, \forall j \in \{2, 3, \dots, s\}$ can be found explicitly from ρ^n, g^n and the previous stage values $\rho^{(l)}, g^{(l)}, \forall l \in \{1, 2, \dots, j-1\}$. Indeed, proceeding similarly as for the first order scheme, we get the following expression of $g^{(j)}, j = 1, \dots, s$ from equation (3.11),

$$g^{(j)} = \mathcal{I}_{\epsilon, \Delta t}^{(j)} \left(\epsilon^2 g^n - \epsilon \sum_{k=1}^{j-1} \tilde{a}_{jk} \Delta t \mathcal{T} g^{(k)} - \epsilon \sum_{k=1}^j a_{jk} \Delta t v M \cdot \nabla_x \rho^{(k)} + \sum_{k=1}^{j-1} a_{jk} \Delta t L g^{(k)} \right). \tag{3.12}$$

Further, we write equation (3.10) by splitting the summation on k as

$$\rho^{(j)} = \rho^n - \sum_{k=1}^{j-1} a_{jk} \frac{\Delta t}{\epsilon} \nabla_x \cdot \langle v g^{(k)} \rangle_V - a_{jj} \frac{\Delta t}{\epsilon} \nabla_x \cdot \langle v g^{(j)} \rangle_V,$$

and inserting equation (3.12) in the last term leads to the update of $\rho^{(j)}$ for $j = 1, \dots, s$

$$\begin{aligned} \rho^{(j)} = & \left(I - a_{jj}^2 \Delta t^2 \nabla_x \cdot \left(\mathcal{D}_{\epsilon, \Delta t}^{(j)} \nabla_x \right) \right)^{-1} \left(\rho^n - \sum_{k=1}^{j-1} a_{jk} \frac{\Delta t}{\epsilon} \nabla_x \cdot \langle v g^{(k)} \rangle_V \right. \\ & - a_{jj} \Delta t \nabla_x \cdot \left\langle v \mathcal{I}_{\epsilon, \Delta t}^{(j)} \left(\epsilon g^n - \sum_{k=1}^{j-1} \tilde{a}_{jk} \Delta t \mathcal{T} g^{(k)} \right. \right. \\ & \left. \left. - \sum_{k=1}^{j-1} a_{jk} \Delta t v M \cdot \nabla_x \rho^{(k)} + \frac{1}{\epsilon} \sum_{k=1}^{j-1} a_{jk} \Delta t L g^{(k)} \right) \right\rangle_V \Big), \end{aligned} \tag{3.13}$$

where the definition of $\mathcal{T}, \mathcal{D}_{\epsilon, \Delta t}^{(j)}$ and $\mathcal{I}_{\epsilon, \Delta t}^{(j)}$ are given by equations (3.7) to (3.9). After this reformulation, $\rho^{(j)}$ can be computed from (3.13) by inverting a linear elliptic type problem and following this, $g^{(j)}$ can be found from equation (3.12). The GSA property in equation (3.5) guarantees that the solution at $t^{n+1} = (n+1)\Delta t$ is same as the last RK stage values, that is, $\rho^{n+1} = \rho^{(s)}$ and $g^{n+1} = g^{(s)}$.

Remark 3.1. The IMEX strategy is similar to the one presented in [33] where the Schur complement is employed to make the scheme efficient from a computational point of view. Here, inserting $g^{(j)}$ in the update (3.13) of $\rho^{(j)}$ leads to a similar scheme.

However, we present here the asymptotic preserving properties of both CK-ARS and type A time integrators and show that the type A time integrators require neither well-prepared initial data nor the treatment of reducing initial time steps as in [33].

4. ASYMPTOTIC PRESERVING PROPERTY

In this section, we show that the time integrated scheme (3.12) and (3.13) becomes a consistent scheme for the diffusion equation (2.5) in the limit $\epsilon \rightarrow 0$. We will discuss the asymptotic preserving property for both CK-ARS and type A time integrators. First, we recall the definition of well-prepared initial data in our context.

Definition 4.1 (Well-prepared initial data). The initial data $\rho(0, x)$ and $g(0, x, v)$ in equations (2.9) and (2.10) are said to be well-prepared if $g(0, x, v) = O(\epsilon)$.

Lemma 4.2. Assume that ϵ is sufficiently small. Let \tilde{a}_{jk} and a_{jk} be the coefficients of the RK method (3.4) applied to the scheme (3.10) and (3.11). Then, the following holds:

- (1) CK-ARS case: If $g^n = O(\epsilon)$, then $g^{(1)} = g^n = O(\epsilon)$ and $g^{(j)} = \epsilon L^{-1}(vM) \cdot \nabla_x \rho^{(j)} + O(\epsilon^2), \forall j \in \{2, \dots, s\}$.

(2) *Type A case:* $g^{(j)} = \epsilon L^{-1}(vM) \cdot \nabla_x \rho^{(j)} + O(\epsilon^2), \forall j \in \{1, \dots, s\}$.

Proof. Let $j \in \{1, \dots, s\}$ such that $a_{jj} \neq 0$. Observe that the operator $\mathcal{I}_{\epsilon, \Delta t}^{(j)}$ defined in (3.9) admits, for small ϵ , the following expansion:

$$\mathcal{I}_{\epsilon, \Delta t}^{(j)} = -(a_{jj} \Delta t L)^{-1} + O(\epsilon^2). \tag{4.1}$$

Consider now an A-type time integrator, so with $a_{jj} \neq 0$ for any $j \in \{1, \dots, s\}$, and assume $g^n = O(1)$. From (3.12) and the previous expansion, we obtain

$$g^{(1)} = -(a_{11} \Delta t L)^{-1} \left[-\epsilon a_{11} \Delta t v M \cdot \nabla_x \rho^{(1)} \right] + O(\epsilon^2) = \epsilon L^{-1}(vM) \cdot \nabla_x \rho^{(1)} + O(\epsilon^2).$$

Now, the proof is performed by induction on $j \in \{2, \dots, s\}$ assuming that for any $k \in \{1, \dots, j-1\}$, $g^{(k)} = \epsilon L^{-1}(vM) \cdot \nabla_x \rho^{(k)} + O(\epsilon^2)$. In particular $g^{(k)} = O(\epsilon)$ and the formula (3.12) has therefore the following expansion:

$$g^{(j)} = -(a_{jj} \Delta t L)^{-1} \left[O(\epsilon^2) - \epsilon \sum_{k=1}^j a_{jk} \Delta t v M \cdot \nabla_x \rho^{(k)} + \sum_{k=1}^{j-1} a_{jk} \Delta t L g^{(k)} \right] + O(\epsilon^2).$$

Inserting the induction hypothesis in the last sum, most of the terms in the two sums eliminate so that finally $g^{(j)} = \epsilon L^{-1}(vM) \cdot \nabla_x \rho^{(j)} + O(\epsilon^2)$.

The case of a CK-ARS time integrator is slightly different. First $a_{11} = 0$ so that $g^{(1)} = g^n = O(\epsilon)$ by the particular well-prepared assumption. Now $a_{22} \neq 0$ and (3.12) has the following expansion for $j = 2$:

$$g^{(2)} = -(a_{22} \Delta t L)^{-1} \left[O(\epsilon^2) - \epsilon a_{22} \Delta t v M \cdot \nabla_x \rho^{(2)} \right] + O(\epsilon^2) = \epsilon L^{-1}(vM) \cdot \nabla_x \rho^{(2)} + O(\epsilon^2).$$

Again, the proof is by induction on $j \in \{3, \dots, s\}$ assuming for any $k \in \{2, \dots, j-1\}$, $g^{(k)} = \epsilon L^{-1}(vM) \cdot \nabla_x \rho^{(k)} + O(\epsilon^2)$. The same computation as above is available since $g^{(1)} = O(\epsilon)$. One has (note that $a_{j1} = 0$ for any j so that the sums start at $k = 2$):

$$\begin{aligned} g^{(j)} &= -(a_{jj} \Delta t L)^{-1} \left[O(\epsilon^2) - \epsilon \sum_{k=2}^j a_{jk} \Delta t v M \cdot \nabla_x \rho^{(k)} + \sum_{k=2}^{j-1} a_{jk} \Delta t L g^{(k)} \right] + O(\epsilon^2) \\ &= \epsilon L^{-1}(vM) \cdot \nabla_x \rho^{(j)} + O(\epsilon^2). \end{aligned}$$

□

Due to the GSA property of both time integrators, we have $g^{n+1} = g^{(s)} = \epsilon L^{-1}(vM) \cdot \nabla_x \rho^{(s)} + O(\epsilon^2) = \epsilon L^{-1}(vM) \cdot \nabla_x \rho^{n+1} + O(\epsilon^2)$ for sufficiently small ϵ . Thus, the following are evident from Lemma 4.2:

- (1) For type CK-ARS, if the initial data is well-prepared (that is, $g^0 = O(\epsilon)$), then $g^n = O(\epsilon), \forall n > 0$.
- (2) For type A, if the initial data is such that $g^0 = O(1)$, then $g^n = O(\epsilon), \forall n > 0$.

As observed in [10], the initial data does not need to be well-prepared for type A time integrator, unlike type CK-ARS, to ensure AP property.

Theorem 4.3. *Consider the scheme (3.10) and (3.11) approximating the macro-micro model (2.7) and (2.8), with the RK method (3.4) of type A or of type CK-ARS (with well-prepared initial data $g^0 = O(\epsilon)$). Then in the limit $\epsilon \rightarrow 0$, the scheme (3.10) and (3.11) degenerates to the following scheme for the diffusion equation*

$$\rho^{(j)} = \rho^n + \sum_{k=1}^j a_{jk} \Delta t \nabla_x \cdot \left(\kappa \nabla_x \rho^{(k)} \right), \forall j = 1, \dots, s, \kappa = -\langle v \otimes L^{-1}(vM) \rangle_V. \tag{4.2}$$

Proof. Corresponding to each case (CK-ARS or type A), we have the following:

Type CK-ARS: assumptions in criterion 1 of Lemma 4.2 are satisfied, and its implications can be utilised. Hence, inserting $g^{(\ell)} = \epsilon L^{-1}(vM) \cdot \nabla_x \rho^{(\ell)} + O(\epsilon^2)$, $\forall \ell \in \{2, 3, \dots, s\}$ into equation (3.10), we get (recall that $a_{j1} = 0$)

$$\begin{aligned} \rho^{(j)} &= \rho^n - \frac{\Delta t}{\epsilon} \sum_{k=2}^j a_{jk} \nabla_x \cdot \left\langle v \epsilon L^{-1}(vM) \cdot \nabla_x \rho^{(k)} \right\rangle_V + O(\epsilon), \\ &= \rho^n - \Delta t \sum_{k=2}^j a_{jk} \nabla_x \cdot \left(\left\langle v \otimes L^{-1}(vM) \right\rangle_V \nabla_x \rho^{(k)} \right) + O(\epsilon). \end{aligned}$$

Type A: assumptions in criterion 2 of Lemma 4.2 are satisfied, and its implications can be utilised. Hence, inserting $g^{(\ell)} = \epsilon L^{-1}(vM) \cdot \nabla_x \rho^{(\ell)} + O(\epsilon^2)$, $\forall \ell \in \{1, 2, \dots, s\}$ into equation (3.10), we get the required result by following the same simplification as before. The only difference is that here $\sum_{k=1}^j$ instead of $\sum_{k=2}^j$. \square

Remark 4.4. For type CK-ARS, if the initial data is not well-prepared, computing $g^{(2)}$ from (3.11) involves $\epsilon \frac{\tilde{a}_{21}}{a_{22}} L^{-1}(I - \Pi)(v \cdot \nabla_x g^{(1)})$ which is not of $O(\epsilon^2)$. Thus,

$$g^{(2)} = \epsilon \frac{\tilde{a}_{21}}{a_{22}} L^{-1}(I - \Pi)(v \cdot \nabla_x g^{(1)}) + \epsilon L^{-1}(vM) \cdot \nabla_x \rho^{(2)} + O(\epsilon^2),$$

and inserting in the macro equation equation (3.10) for $j = 2$ leads to (since $a_{21} = 0$)

$$\rho^{(2)} = \rho^n - \frac{\tilde{a}_{21}}{a_{22}} \Delta t \left\langle v \otimes L^{-1} \left((I - \Pi) v \nabla_x^2 g^{(1)} \right) \right\rangle_V - a_{22} \Delta t \nabla_x \cdot \left(\left\langle v \otimes L^{-1}(vM) \right\rangle_V \nabla_x \rho^{(2)} \right) + O(\epsilon),$$

which is not consistent with the diffusion equation. Thus, for CK-ARS, asymptotic consistency cannot be attained if the initial data is not well-prepared.

5. SPACE AND VELOCITY DISCRETIZATION

In this section, we present the spatial (for both non-staggered and staggered grids) and velocity discretization strategies that we employ in our numerical scheme.

5.1. Discrete velocity method

For the velocity discretization, we will follow the discrete velocity method [20]. Thus, the velocity domain is truncated as $v \in [-v_{\max}, v_{\max}]$, and a uniform mesh is used $v_k = -v_{\max} + k\Delta v$, $k = 1, \dots, N_v$ ($N_v \in \mathbb{N}^*$) and $\Delta v = 2v_{\max}/N_v$. Further, $f(t, x, v)$ and $M(v)$ are represented as:

$$f_k(t, x) := f(t, x, v_k), \quad M_k := M(v_k) \quad \text{for } k = 1, \dots, N_v.$$

Then, according to the definitions (2.3) and (2.6), we have for $j = 1, \dots, N_v$

$$\rho(t, x) \approx \frac{\sum_{k=0}^{N_v-1} f_k \Delta v}{\sum_{k=0}^{N_v-1} M_k \Delta v} \quad \text{and} \quad (\Pi f(t, x, v))_j \approx \frac{\sum_{k=0}^{N_v-1} f_k \Delta v}{\sum_{k=0}^{N_v-1} M_k \Delta v} M_j.$$

For the presentation, we will keep velocity continuous to focus on space discretization.

5.2. Space discretization using staggered grid

First, we will consider staggered grid to approximate $g^{(j)}$ and $\rho^{(j)}$ in space following [30]: the two meshes of the space interval $[0, 1]$ are $x_i = i\Delta x$ and $x_{i+1/2} = (i + 1/2)\Delta x$ for $i = 0, \dots, N_x$ ($N_x \in \mathbb{N}^*$), with $\Delta x = L/N_x$. Periodic boundary conditions will be considered in this section.

The expressions for $g^{(j)}$ and $\rho^{(j)}$ in (3.12) and (3.13) are spatially discretised by considering staggered grid: $\rho^{(j)}$ is stored at x_i ($\rho_i^{(j)} \approx \rho^{(j)}(x_i)$), and $g^{(j)}$ is stored at $x_{i+1/2}$ ($g_{i+1/2}^{(j)}(v) \approx g^{(j)}(x_{i+1/2}, v)$). The term $v \cdot \nabla_x g^{(k)}$ in (3.12) and (3.13) is discretised in an upwind fashion as $v \cdot \nabla_x \approx v^+ \cdot \mathbf{G}_{\text{upw}}^- + v^- \cdot \mathbf{G}_{\text{upw}}^+$ where $v^\pm = (v \pm |v|)/2$, $\mathbf{G}_{\text{upw}}^\pm$ denote the $N_x \times N_x$ matrices that approximate ∇_x . For instance, the first order version is

$$\mathbf{G}_{\text{upw}}^- = \frac{1}{\Delta x} \text{circ}([-1, \underline{1}]), \quad \mathbf{G}_{\text{upw}}^+ = \frac{1}{\Delta x} \text{circ}([\underline{-1}, 1]), \quad (5.1)$$

where the notation circ is defined in Appendix A. With these notations, we get

$$\left(v \partial_x g^{(j)} \right)_{x_{i+1/2}} \approx v^+ \frac{g_{i+\frac{1}{2}}^{(j)} - g_{i-\frac{1}{2}}^{(j)}}{\Delta x} + v^- \frac{g_{i+\frac{3}{2}}^{(j)} - g_{i+\frac{1}{2}}^{(j)}}{\Delta x} = \left((v^+ \mathbf{G}_{\text{upw}}^- + v^- \mathbf{G}_{\text{upw}}^+) g^{(j)} \right)_i,$$

where in the last term, the i index has to be understood as the i -th component of the vector. Instead of first order upwind discretization, one can also use high order upwind discretizations so that the matrices $\mathbf{G}_{\text{upw}}^\pm$ will be different. Further, the term $vM \cdot \nabla_x \rho^{(k)}$ in (3.12), (3.13) and the terms of the form $\nabla_x \cdot \langle (\cdot) \rangle_V$ in (3.13) are discretised using second order central differences as in [30]. In particular, the term $vM \cdot \nabla_x \rho^{(k)}$ is approximated by

$$\left(vM \partial_x \rho^{(k)} \right)_{x_{i+1/2}} \approx vM \frac{\rho_{i+1}^{(k)} - \rho_i^{(k)}}{\Delta x} = \left(vM \mathbf{G}_{\text{cen}_g} \rho^{(k)} \right)_i, \quad \mathbf{G}_{\text{cen}_g} = \frac{1}{\Delta x} \text{circ}([-1, 1]). \quad (5.2)$$

Finally, the gradient terms $\nabla_x \cdot \langle (\cdot) \rangle_V$ in (3.13) are approximated as follows

$$\left(\partial_x \langle \cdot \rangle_V \right)_{x_i} = \frac{\langle \cdot \rangle_{V, i+1/2} - \langle \cdot \rangle_{V, i-1/2}}{\Delta x} = \left(\mathbf{G}_{\text{cen}_\rho} \langle \cdot \rangle_V \right)_i, \quad \mathbf{G}_{\text{cen}_\rho} = \frac{1}{\Delta x} \text{circ}([-1, \underline{1}]). \quad (5.3)$$

Again, high order centered finite differences methods can be used so that it will give different expressions for $\mathbf{G}_{\text{cen}_\rho}$ and $\mathbf{G}_{\text{cen}_g}$. Let us remark that the term $\nabla_x \cdot \nabla_x = \nabla_x^2$ in (3.13) is approximated by $\mathbf{G}_{\text{cen}_\rho} \mathbf{G}_{\text{cen}_g}$, *i.e.*, $\mathbf{G}_{\text{cen}_\rho} \mathbf{G}_{\text{cen}_g} = \frac{1}{\Delta x^2} \text{circ}([1, \underline{-2}, 1])$, which gives the standard second order approximation of the Laplacian.

To ease the reading, we present the fully discrete scheme for first order ARS(1, 1, 1) but the generalization to high order can be done using the elements of Section 3

$$\begin{aligned} g^{n+1} &= (\epsilon^2 I - \Delta t L)^{-1} (\epsilon^2 g^n - \epsilon \Delta t (I - \Pi) (v^+ \mathbf{G}_{\text{upw}}^- + v^- \mathbf{G}_{\text{upw}}^+) g^n - \epsilon \Delta t v M \mathbf{G}_{\text{cen}_g} \rho^{n+1}) \\ \rho^{n+1} &= \left(I - \Delta t^2 \mathbf{G}_{\text{cen}_\rho} \left(\left\langle v \otimes (\epsilon^2 I - \Delta t L)^{-1} (vM) \right\rangle_V \mathbf{G}_{\text{cen}_g} \right) \right)^{-1} \\ &\quad \times \left(\rho^n - \Delta t \mathbf{G}_{\text{cen}_\rho} \left\langle v (\epsilon^2 I - \Delta t L)^{-1} (\epsilon g^n - \Delta t (I - \Pi) ((v^+ \mathbf{G}_{\text{upw}}^- + v^- \mathbf{G}_{\text{upw}}^+) g^n)) \right\rangle_V \right). \end{aligned}$$

5.3. Space discretization using non-staggered grid

We also address the case of non-staggered grids which may be more appropriate when high dimensions are considered in space since only one spatial mesh is used: $x_i = i\Delta x$, for $i = 0, 1, \dots, N_x$, with $\Delta x = L/N_x$. Let $g^{(j)}$ and $\rho^{(j)}$ in (3.12) and (3.13) $\forall j \in \{1, 2, \dots, s\}$ be approximated in space by $g_i^{(j)}(v) \approx g^{(j)}(x_i, v)$ and $\rho_i^{(j)} \approx \rho^{(j)}(x_i)$. The term $v \cdot \nabla_x g^{(k)}$ in (3.12) and (3.13) is discretised in an upwind fashion as $v \cdot \nabla_x = v^+ \mathbf{G}_{\text{upw}}^- + v^- \mathbf{G}_{\text{upw}}^+$, where $v^\pm = (v \pm |v|)/2$. Here, $\mathbf{G}_{\text{upw}}^\pm$ denote the matrices that represent an upwind approximation of ∇_x . For instance, the definition (5.1) can be used, but also its third order version

$$\mathbf{G}_{\text{upw}}^- = \frac{1}{6\Delta x} \text{circ}([1, -6, \underline{3}, 2]), \quad \mathbf{G}_{\text{upw}}^+ = \frac{1}{6\Delta x} \text{circ}([-2, \underline{-3}, 6, -1]), \quad (5.4)$$

where circ represents the matrix notation described in Appendix A can be used. The term $vM \cdot \nabla_x \rho^{(k)}$ in (3.12), (3.13) and the terms of the form $\nabla_x \cdot \langle (\cdot) \rangle_V$ in (3.13) are discretised in central fashion, since these terms act as source in equation (3.12) and diffusion in (3.13). Here, ∇_x is approximated by central differences as in (5.3) or (5.2) but in the non-staggered case, the same matrix can be used for both terms. As an example, the fourth order central difference produces:

$$\mathbf{G}_{\text{cen}} = \frac{1}{12\Delta x} \text{circ}([1, -8, \underline{0}, 8, -1]). \quad (5.5)$$

The term $\nabla_x \cdot \nabla_x = \nabla_x^2$ in (3.13) is discretised as the matrices product $\mathbf{G}_{\text{cen}}^2 = \mathbf{G}_{\text{cen}} \mathbf{G}_{\text{cen}}$. Like in the staggered grid case, we present the fully discrete scheme for first order ARS(1, 1, 1) time discretization to ease the reading:

$$\begin{aligned} g^{n+1} &= (\epsilon^2 I - \Delta t L)^{-1} (\epsilon^2 g^n - \epsilon \Delta t (I - \Pi) (v^+ \mathbf{G}_{\text{upw}}^- + v^- \mathbf{G}_{\text{upw}}^+) g^n - \epsilon \Delta t v M \mathbf{G}_{\text{cen}} \rho^{n+1}) \\ \rho^{n+1} &= \left(I - \Delta t^2 \mathbf{G}_{\text{cen}} \left(\left\langle v \otimes (\epsilon^2 I - \Delta t L)^{-1} (v M) \right\rangle_V \mathbf{G}_{\text{cen}} \right) \right)^{-1} \\ &\quad \times \left(\rho^n - \Delta t \mathbf{G}_{\text{cen}} \left\langle v (\epsilon^2 I - \Delta t L)^{-1} (\epsilon g^n - \Delta t (I - \Pi) ((v^+ \mathbf{G}_{\text{upw}}^- + v^- \mathbf{G}_{\text{upw}}^+) g^n)) \right\rangle_V \right). \end{aligned}$$

Remark 5.1. We know that the term $\sum_{k=1}^j a_{jk} \frac{\Delta t}{\epsilon} \nabla_x \cdot \langle v g^{(k)} \rangle_V$ in (3.10) is split into first $j-1$ and last j contributions, and $g^{(j)}$ is substituted for the last j contribution, as in (3.13). The gradient in $\sum_{k=1}^{j-1} a_{jk} \frac{\Delta t}{\epsilon} \nabla_x \cdot \langle v g^{(k)} \rangle_V$ of (3.13) is discretised using $\mathbf{G}_{\text{cen}_\rho}$. Further, the substitution of $g^{(j)}$ for the last j hints the combination of $\nabla_x \cdot \nabla_x$ as ∇_x^2 for the terms of $g^{(j)}$ involving $\nabla_x g$ and $\nabla_x \rho$. However, if we choose a spatial discretization for ∇_x^2 as \mathbf{G}_{diff} , then these terms will experience $\mathbf{G}_{\text{cen}_\rho} \mathbf{G}_{\text{cen}_g}$ for the first $j-1$ contributions and \mathbf{G}_{diff} for the last j contribution of the $\rho^{(j)}$ update equation. This disrupts the ODE structure present in RK time discretization, and hence reduction to first order time accuracy was observed numerically. Therefore, in order to retain high order time accuracy, it is important to carry out the space discretization carefully. Hence, we do not introduce a different discretization for ∇_x^2 , and we retain $\mathbf{G}_{\text{cen}_\rho} \mathbf{G}_{\text{cen}_g}$ even for the last j contribution of $\rho^{(j)}$ equation.

Remark 5.2. The matrices introduced for spatial discretization do not change the Chapman–Enskog expansion so that the AP property is still true in the fully discrete form. Thus, we have $g^{(k)} = \epsilon L^{-1} (v M) \mathbf{G}_{\text{cen}_g} \rho^{(k)} + O(\epsilon^2)$ for $k \in \{1, \dots, s\}$ by using type A. For CK-ARS with well-prepared data, we have $g^{(k)} = \epsilon L^{-1} (v M) \mathbf{G}_{\text{cen}_g} \rho^{(k)} + O(\epsilon^2)$ for $k \in \{2, \dots, s\}$. Inserting this in macro equation, we get the corresponding RK scheme for the diffusion

$$\rho^{(j)} = \rho^n - \Delta t \sum_{k=1}^j a_{jk} \mathbf{G}_{\text{cen}_\rho} \left(\left\langle v \otimes L^{-1} (v M) \right\rangle_V \mathbf{G}_{\text{cen}_g} \rho^{(k)} \right) + O(\epsilon).$$

6. EXTENSIONS TO ADVECTION-DIFFUSION COLLISION OPERATOR AND INFLOW BOUNDARY PROBLEMS

In this section, we show that our high order AP schemes can be extended to other problems involving advection-diffusion asymptotics and inflow boundaries.

6.1. Advection-diffusion asymptotics

In this part, an advection-diffusion collision operator is considered (see [17, 21]),

$$\mathcal{L}f := Lf + \epsilon v M \cdot A \langle f \rangle_V, \quad A \in \mathbb{R}^d, \quad |\epsilon A| < 1, \quad (6.1)$$

where L denotes a collision satisfying the properties listed in Section 2. A famous simple example is $Lf = \langle f \rangle_V M - f$.

Using the notations introduced in Section 2, we can derive the micro-macro model satisfied by $\rho = \langle f \rangle_V$ and $g = f - \rho M$ by applying Π and $I - \Pi$ to equation (2.1) with collision \mathcal{L} to get the macro and micro equations in this context

$$\partial_t \rho + \frac{1}{\epsilon} \nabla_x \cdot \langle v g \rangle_V = 0, \tag{6.2}$$

$$\partial_t g + \frac{1}{\epsilon} (I - \Pi)(v \cdot \nabla_x g) + \frac{1}{\epsilon} v M \cdot \nabla_x \rho = \frac{1}{\epsilon^2} L g + \frac{1}{\epsilon} v M \cdot A \rho. \tag{6.3}$$

A Chapman–Enskog expansion can be performed to get $g = \epsilon L^{-1}(vM) \cdot \nabla_x \rho - \epsilon L^{-1}(vM) \cdot A \rho + \mathcal{O}(\epsilon^2)$. Inserting this in the macro equation (6.2) enables to obtain an advection-diffusion equation in the limit $\epsilon \rightarrow 0$:

$$\partial_t \rho + \nabla_x \cdot (\langle v \otimes L^{-1}(vM) \rangle_V \nabla_x \rho) - \nabla_x \cdot (\langle v \otimes L^{-1}(vM) \rangle_V A \rho) = 0. \tag{6.4}$$

The goal is to design a uniformly stable high order time integrators for (6.2) and (6.3) so that they degenerate into a high order time integrator for (6.4) as $\epsilon \rightarrow 0$. The extension of the schemes introduced in Section 3 will lead to an IMEX discretization of the asymptotic model (6.4), where the advection term is treated explicitly while the diffusion term is implicit.

6.1.1. High order time integrator

In this subsection, we present the discretization of macro and micro equations (6.2) and (6.3). As in Section 3, in the micro equation, we treat $\frac{1}{\epsilon^2} L g$ implicitly to ensure uniform stability and the additional term $\frac{1}{\epsilon} v M \cdot A \rho$ explicitly since it will be stabilized by the implicit treatment of the stiffest term. Regarding the macro equation and the remaining terms in micro equation, we follow the lines from previous Section 3. We thus obtain the following high order IMEX RK scheme to approximate (6.2) and (6.3)

$$\rho^{(j)} = \rho^n - \sum_{k=1}^j a_{jk} \frac{\Delta t}{\epsilon} \nabla_x \cdot \langle v g^{(k)} \rangle_V, \tag{6.5}$$

$$g^{(j)} = g^n - \frac{\Delta t}{\epsilon} \left[\sum_{k=1}^{j-1} \tilde{a}_{jk} \mathcal{T} g^{(k)} + \sum_{k=1}^j a_{jk} v M \cdot \nabla_x \rho^{(k)} - \sum_{k=1}^j \frac{a_{jk}}{\epsilon} L g^{(k)} - \sum_{k=1}^{j-1} \tilde{a}_{jk} v M \cdot A \rho^{(k)} \right], \tag{6.6}$$

where the coefficients a_{jk}, \tilde{a}_{jk} are given by the Butcher tableaux. As in Section 3, some calculations are required to make the algorithm explicit. First, we have

$$g^{(j)} = \mathcal{I}_{\epsilon, \Delta t}^{(j)} \left(\epsilon^2 g^n - \epsilon \Delta t \left[\sum_{k=1}^{j-1} \tilde{a}_{jk} \mathcal{T} g^{(k)} + \sum_{k=1}^j a_{jk} v M \cdot \nabla_x \rho^{(k)} - \frac{1}{\epsilon} \sum_{k=1}^{j-1} a_{jk} L g^{(k)} - \sum_{k=1}^{j-1} \tilde{a}_{jk} v M \cdot A \rho^{(k)} \right] \right), \tag{6.7}$$

with $\mathcal{T} g^{(k)} = (I - \Pi)(v \cdot \nabla_x g^{(k)})$ and $\mathcal{I}_{\epsilon, \Delta t}^{(j)} = (\epsilon^2 I - a_{jj} \Delta t L)^{-1}$. Then, $\rho^{(j)}$ is obtained by inserting $g^{(j)}$ given by (6.7) in the macro equation (6.5) to get

$$\begin{aligned} \rho^{(j)} = & \left(I - a_{jj}^2 \Delta t^2 \nabla_x \cdot \left(\mathcal{D}_{\epsilon, \Delta t}^{(j)} \nabla_x \right) \right)^{-1} \left(\rho^n - \sum_{k=1}^{j-1} a_{jk} \frac{\Delta t}{\epsilon} \nabla_x \cdot \langle v g^{(k)} \rangle_V \right. \\ & - a_{jj} \Delta t \nabla_x \cdot \left\langle v \mathcal{I}_{\epsilon, \Delta t}^{(j)} \left(\epsilon g^n - \sum_{k=1}^{j-1} \tilde{a}_{jk} \Delta t \mathcal{T} g^{(k)} - \sum_{k=1}^{j-1} a_{jk} \Delta t v M \cdot \nabla_x \rho^{(k)} \right. \right. \\ & \left. \left. + \frac{1}{\epsilon} \sum_{k=1}^{j-1} a_{jk} \Delta t L g^{(k)} + \sum_{k=1}^{j-1} \tilde{a}_{jk} \Delta t v M \cdot A \rho^{(k)} \right) \right\rangle_V \left. \right), \end{aligned} \tag{6.8}$$

where $\mathcal{D}_{\epsilon, \Delta t}^{(j)} = \langle v \otimes (\epsilon^2 I - a_{jj} \Delta t L)^{-1}(vM) \rangle_V$. Thus, $\rho^{(j)}$ can be updated by using (6.8) and $g^{(j)}$ can be found explicitly by using (6.7).

6.1.2. Asymptotic preserving property

This part is dedicated to the asymptotic preserving property of the scheme (6.7) and (6.8). We first show the AP property of type A time integrator, and we later remark how this property is true for the CK-ARS time integrator with well-prepared initial data. First we have

Lemma 6.1. *If $g^n = O(1)$ and $g^{(k)} = O(\epsilon), \forall k \in \{1, 2, \dots, j-1\}$, then $g^{(j)} = O(\epsilon), \forall j \in \{2, 3, \dots, s\}$ for small ϵ . In particular, we have $\forall j \in \{2, 3, \dots, s\}$*

$$g^{(j)} = \epsilon \sum_{k=1}^j \frac{a_{jk}}{a_{jj}} L^{-1}(vM) \cdot \nabla_x \rho^{(k)} - \sum_{k=1}^{j-1} \frac{a_{jk}}{a_{jj}} g^{(k)} - \epsilon \sum_{k=1}^{j-1} \frac{\tilde{a}_{jk}}{a_{jj}} L^{-1}(vM) \cdot A\rho^{(k)} + O(\epsilon^2). \tag{6.9}$$

Proof. Plugging in equation (6.7) the expansion (4.1) of $\mathcal{T}_{\epsilon, \Delta t}^{(j)}$ given by equation (3.9), along with the assumptions stated in the lemma, we obtain (6.9) from which we deduce $g^{(j)} = O(\epsilon)$ for all $j \in \{2, 3, \dots, s\}$. \square

Remark 6.2. For type A time integrator, if $g^n = O(1)$, we have from (6.7):

$$g^{(1)} = \epsilon \frac{a_{11}}{a_{11}} vM \cdot \nabla_x \rho^{(1)} + O(\epsilon^2) = O(\epsilon).$$

This satisfies the induction hypothesis in Lemma 6.1. Further, equation (6.9) holds by omitting $\sum_{k=1}^{j-1}$ terms for $j = 1$. Thus, equation (6.9) is true for $j \in \{1, 2, \dots, s\}$.

Lemma 6.1 enables to get an expansion of $g^{(j)}$ that can be inserted in (6.8) to identify the time discretization of the asymptotic limit. However, this leads to quite involved calculations which requires to introduce some notations.

Definition 6.3. For $j \in \{1, 2, \dots, s\}$ and $k_1, m \in \{1, 2, \dots, j\}$ we define

$$\Pi_{j, k_1}^m = \left\langle v \frac{a_{jk_1}}{a_{k_1 k_1}} (\mathcal{S}^{k_0} \mathcal{S}^{k_1} \mathcal{S}^{k_2} \dots \mathcal{S}^{k_{m-1}}) (\mathcal{R}^{k_m}) \right\rangle_V, \tag{6.10}$$

with

$$\begin{aligned} \mathcal{S}^{k_0} &= 1, & \mathcal{S}^{k_l} &= \sum_{k_{l+1}=1}^{k_l-1} \frac{a_{k_l k_{l+1}}}{a_{k_{l+1} k_{l+1}}} \text{ for } l \in \{1, 2, \dots, m-1\}, \quad m \geq 2, \\ \mathcal{R}^{k_m} &= \sum_{k_{m+1}=1}^{k_m} a_{k_m k_{m+1}} L^{-1}(vM) \cdot \nabla_x \rho^{(k_{m+1})} - \sum_{k_{m+1}=1}^{k_m-1} \tilde{a}_{k_m k_{m+1}} L^{-1}(vM) \cdot A\rho^{(k_{m+1})}. \end{aligned}$$

As usual, we will use the convention $\sum_{j=1}^q \equiv 0$ if $q \in \mathbb{Z} \setminus \mathbb{N}$.

The term Π_{j, k_1}^m will be useful in the following study and deserves some remarks: the index m denotes the depth of the embedded sums, j corresponds to the current stage and k_1 corresponds to the indexing over previous stages. We continue with the following lemma which gives an induction relation on Π_{j, k_1}^m .

Lemma 6.4. *For $j \geq 2$, we have*

$$\Pi_{j, j}^m = \sum_{k_1=1}^{j-1} \Pi_{j, k_1}^{m-1} \text{ for } m \in \{2, 3, \dots, j\}, \text{ and } \Pi_{j, k_1}^j = 0 \text{ for } k_1 \in \{1, 2, \dots, j-1\}.$$

Proof. For the first relation, considering $k_1 = j$ (with $j \geq 2$) in (6.10) leads to

$$\Pi_{j,j}^m = \langle v(\mathcal{S}^{k_0} \mathcal{S}^j \mathcal{S}^{k_2} \dots \mathcal{S}^{k_{m-1}})(\mathcal{R}^{k_m}) \rangle_V,$$

since $a_{jj} \neq 0$. Further, since $\mathcal{S}^{k_1=j} = \sum_{k_2=1}^{j-1} \frac{a_{jk_2}}{a_{k_2k_2}}$, we get

$$\Pi_{j,j}^m = \left\langle v \sum_{k_2=1}^{j-1} \frac{a_{jk_2}}{a_{k_2k_2}} (\mathcal{S}^{k_0} \mathcal{S}^{k_2} \dots \mathcal{S}^{k_{m-1}})(\mathcal{R}^{k_m}) \right\rangle_V.$$

By employing the change of variables as $k_\ell \rightarrow k_{\ell-1}$ for $\ell \in \{2, 3, \dots, m\}$ in the right hand side of above expression, we get

$$\begin{aligned} \Pi_{j,j}^m &= \left\langle v \sum_{k_1=1}^{j-1} \frac{a_{jk_1}}{a_{k_1k_1}} (\mathcal{S}^{k_0} \mathcal{S}^{k_1} \dots \mathcal{S}^{k_{m-2}})(\mathcal{R}^{k_{m-1}}) \right\rangle_V \\ &= \sum_{k_1=1}^{j-1} \left\langle v \frac{a_{jk_1}}{a_{k_1k_1}} (\mathcal{S}^{k_0} \mathcal{S}^{k_1} \dots \mathcal{S}^{k_{m-2}})(\mathcal{R}^{k_{m-1}}) \right\rangle_V = \sum_{k_1=1}^{j-1} \Pi_{j,k_1}^{m-1}, \end{aligned}$$

which proves the first identity.

For the second relation, considering $m = j$ in eq. 6.10 leads to

$$\Pi_{j,k_1}^j = \left\langle v \frac{a_{jk_1}}{a_{k_1k_1}} (\mathcal{S}^{k_0} \mathcal{S}^{k_1} \mathcal{S}^{k_2} \dots \mathcal{S}^{k_{j-1}})(\mathcal{R}^{k_j}) \right\rangle_V.$$

We first prove the relation for $j = 2$. It is clear from Definition 6.3 that the summation in \mathcal{S}^{k_1} goes from $k_2 = 1$ to $k_2 = k_1 - 1$. For $k_1 = 1$, the summation goes to $k_2 = k_1 - 1 = 0$. Thus, since \mathcal{S}^{k_1} involves \sum_1^0 for $k_1 = 1$, it is zero according to the convention. Hence $\Pi_{j,k_1}^j = 0$ for $k_1 = 1$.

We now prove the relation for $j > 2$. From Definition 6.3, it can be seen that the summations in \mathcal{S}^{k_1} and \mathcal{S}^{k_2} go from $k_2 = 1$ to $k_2 = k_1 - 1$ and $k_3 = 1$ to $k_3 = k_2 - 1$ respectively. Thus, the summation in \mathcal{S}^{k_2} can go to atmost $k_3 = k_2 - 1 = (k_1 - 1) - 1 = k_1 - 2$. Proceeding in this manner, we see that the summation in $\mathcal{S}^{k_{j-1}}$ can go to atmost $k_j = k_1 - (j - 1)$.

For $k_1 \in \{1, 2, \dots, j-1\}$, $k_j = k_1 - (j-1) \in \mathbb{Z} \setminus \mathbb{N}$ so that $\mathcal{S}^{k_{j-1}} = 0$ and hence $\Pi_{j,k_1}^j = 0$ for $k_1 \in \{1, 2, \dots, j-1\}$ which ends the proof. \square

Now, we can use the previous lemma to identify the asymptotic numerical scheme.

Lemma 6.5. *When $\epsilon \rightarrow 0$, the numerical scheme (6.5) and (6.6) degenerates into*

$$\rho^{(j)} = \rho^n + \Delta t \sum_{k_1=1}^j \nabla_x \cdot \left(\sum_{\ell=1}^j (-1)^\ell \Pi_{j,k_1}^\ell \right) \quad \text{for } j \in \{1, 2, \dots, s\}, \tag{6.11}$$

where Π_{j,k_1}^ℓ is given by Definition 6.3.

Proof. We start with the macro equation in equation (6.5)

$$\rho^{(j)} = \rho^n - \sum_{k_1=1}^j a_{jk_1} \frac{\Delta t}{\epsilon} \nabla_x \cdot \langle v g^{(k_1)} \rangle_V,$$

in which we insert $g^{(k_1)}$ given by equation (6.9) to get

$$\begin{aligned} \rho^{(j)} &= \rho^n - \Delta t \sum_{k_1=1}^j \nabla_x \cdot \left\langle v \frac{a_{jk_1}}{a_{k_1k_1}} \left(\sum_{k_2=1}^{k_1} a_{k_1k_2} L^{-1}(vM) \cdot \nabla_x \rho^{(k_2)} - \sum_{k_2=1}^{k_1-1} \tilde{a}_{k_1k_2} L^{-1}(vM) \cdot A\rho^{(k_2)} \right) \right\rangle_V \\ &\quad + \frac{\Delta t}{\epsilon} \sum_{k_1=1}^j \nabla_x \cdot \left\langle v \frac{a_{jk_1}}{a_{k_1k_1}} \left(\sum_{k_2=1}^{k_1-1} a_{k_1k_2} g^{(k_2)} \right) \right\rangle_V + O(\epsilon) \\ &= \rho^n - \Delta t \sum_{k_1=1}^j \nabla_x \cdot \left\langle v \frac{a_{jk_1}}{a_{k_1k_1}} (\mathcal{S}^{k_0} \mathcal{R}^{k_1}) \right\rangle_V + \frac{\Delta t}{\epsilon} \sum_{k_1=1}^j \nabla_x \cdot \left\langle v \frac{a_{jk_1}}{a_{k_1k_1}} \left(\sum_{k_2=1}^{k_1-1} a_{k_1k_2} g^{(k_2)} \right) \right\rangle_V + O(\epsilon) \\ &= \rho^n - \Delta t \sum_{k_1=1}^j \nabla_x \cdot \Pi_{j,k_1}^1 + \frac{\Delta t}{\epsilon} \sum_{k_1=1}^j \nabla_x \cdot \left\langle v \frac{a_{jk_1}}{a_{k_1k_1}} \left(\sum_{k_2=1}^{k_1-1} a_{k_1k_2} g^{(k_2)} \right) \right\rangle_V + O(\epsilon). \end{aligned}$$

Inserting $g^{(k_2)}$ from equation (6.9) in the above equation and simplifying as before, we get,

$$\rho^{(j)} = \rho^n - \Delta t \sum_{k_1=1}^j \nabla_x \cdot (\Pi_{j,k_1}^1 - \Pi_{j,k_1}^2) - \frac{\Delta t}{\epsilon} \sum_{k_1=1}^j \nabla_x \cdot \left\langle v \frac{a_{jk_1}}{a_{k_1k_1}} \left(\sum_{k_2=1}^{k_1-1} \frac{a_{k_1k_2}}{a_{k_2k_2}} \sum_{k_3=1}^{k_2-1} a_{k_2k_3} g^{(k_3)} \right) \right\rangle_V + O(\epsilon).$$

This procedure can be continued $(j - 1)$ times to finally get,

$$\begin{aligned} \rho^{(j)} &= \rho^n + \Delta t \sum_{k_1=1}^j \nabla_x \cdot \left(\sum_{\ell=1}^{j-1} (-1)^\ell \Pi_{j,k_1}^\ell \right) \\ &\quad - (-1)^{j-1} \frac{\Delta t}{\epsilon} \sum_{k_1=1}^j \nabla_x \cdot \left\langle v \frac{a_{jk_1}}{a_{k_1k_1}} \left(\sum_{k_2=1}^{k_1-1} \frac{a_{k_1k_2}}{a_{k_2k_2}} \dots \sum_{k_{j-1}=1}^{k_{j-2}-1} \frac{a_{k_{j-2}k_{j-1}}}{a_{k_{j-1}k_{j-1}}} \sum_{k_j=1}^{k_{j-1}-1} a_{k_{j-1}k_j} g^{(k_j)} \right) \right\rangle_V + O(\epsilon) \\ &= \rho^n + \Delta t \sum_{k_1=1}^j \nabla_x \cdot \left(\sum_{\ell=1}^{j-1} (-1)^\ell \Pi_{j,k_1}^\ell \right) \\ &\quad - (-1)^{j-1} \frac{\Delta t}{\epsilon} \sum_{k_1=1}^j \nabla_x \cdot \left\langle v \frac{a_{jk_1}}{a_{k_1k_1}} \left(\mathcal{S}^{k_0} \mathcal{S}^{k_1} \dots \mathcal{S}^{k_{j-2}} \sum_{k_j=1}^{k_{j-1}-1} a_{k_{j-1}k_j} g^{(k_j)} \right) \right\rangle_V + O(\epsilon). \end{aligned}$$

We know from Definition 6.3 that the summations in \mathcal{S}^{k_1} and \mathcal{S}^{k_2} go from $k_2 = 1$ to $k_2 = k_1 - 1$ and $k_3 = 1$ to $k_3 = k_2 - 1$ respectively. Thus, the summation in \mathcal{S}^{k_2} can go to atmost $k_3 = k_2 - 1 = (k_1 - 1) - 1 = k_1 - 2$. Proceeding in this manner, we see that the summations in $\mathcal{S}^{k_{j-2}}$ and $\sum_{k_j=1}^{k_{j-1}-1} a_{k_{j-1}k_j} g^{(k_j)}$ go to atmost $k_{j-1} = k_1 - (j - 2)$ and $k_j = k_1 - (j - 1)$ respectively.

Since the summation in k_1 goes to atmost j in the above equation, k_j in the term $\sum_{k_j=1}^{k_{j-1}-1} a_{k_{j-1}k_j} g^{(k_j)}$ goes to atmost $k_j = k_1 - (j - 1) = j - (j - 1) = 1$, and k_{j-1} in $\mathcal{S}^{k_{j-2}}$ goes to atmost $k_{j-1} = k_1 - (j - 2) = j - (j - 2) = 2$ and so on. Thus, only $k_j = 1$ remains in the last summation so that $\sum_{k_j=1}^{k_{j-1}-1} a_{k_{j-1}k_j} g^{(k_j)} = a_{21} g^{(1)} = \epsilon a_{21} L^{-1}(vM) \cdot \nabla_x \rho^{(1)} + O(\epsilon^2) = \frac{a_{21}}{a_{11}} \epsilon a_{11} L^{-1}(vM) \cdot \nabla_x \rho^{(1)} + O(\epsilon^2) = \epsilon \mathcal{S}^{k_{j-1}} \mathcal{R}^{k_j} + O(\epsilon^2)$. Thus, we have

$$\begin{aligned} \rho^{(j)} &= \rho^n + \Delta t \sum_{k_1=1}^j \nabla_x \cdot \left(\sum_{\ell=1}^{j-1} (-1)^\ell \Pi_{j,k_1}^\ell \right) \\ &\quad - (-1)^{j-1} \Delta t \sum_{k_1=1}^j \nabla_x \cdot \left\langle v \frac{a_{jk_1}}{a_{k_1k_1}} (\mathcal{S}^{k_0} \mathcal{S}^{k_1} \dots \mathcal{S}^{k_{j-1}} \mathcal{R}^{k_j}) \right\rangle_V + O(\epsilon) \end{aligned}$$

$$= \rho^n + \Delta t \sum_{k_1=1}^j \left[\nabla_x \cdot \left(\sum_{\ell=1}^{j-1} (-1)^\ell \Pi_{j,k_1}^\ell \right) + \nabla_x \cdot \left((-1)^j \Pi_{j,k_1}^j \right) \right] + O(\epsilon).$$

□

We can now prove the asymptotic property of the scheme (6.5) and (6.6).

Theorem 6.6. *When $\epsilon \rightarrow 0$, the scheme (6.5) and (6.6) degenerates into*

$$\begin{aligned} \rho^{(j)} &= \rho^n - \Delta t \sum_{k=1}^j a_{jk} \nabla_x \cdot \left(\langle v \otimes L^{-1}(vM) \rangle_V \nabla_x \rho^{(k)} \right) \\ &\quad + \Delta t \sum_{k=1}^{j-1} \tilde{a}_{jk} \nabla_x \cdot \left(\langle v \otimes L^{-1}(vM) \rangle_V A \rho^{(k)} \right), \quad \text{for } j \in \{1, 2, \dots, s\}. \end{aligned} \tag{6.12}$$

Proof. From Lemma 6.5, the asymptotic limit $\epsilon \rightarrow 0$ of the macro equation in equation (6.5) is (for $j \in \{1, 2, \dots, s\}$)

$$\begin{aligned} \rho^{(j)} &= \rho^n + \Delta t \sum_{k_1=1}^j \nabla_x \cdot \left(\sum_{\ell=1}^j (-1)^\ell \Pi_{j,k_1}^\ell \right) = \rho^n + \Delta t \nabla_x \cdot \left(\sum_{\ell=1}^j (-1)^\ell \left(\Pi_{j,j}^\ell + \sum_{k_1=1}^{j-1} \Pi_{j,k_1}^\ell \right) \right) \\ &= \rho^n + \Delta t \nabla_x \cdot \left(-\Pi_{j,j}^1 + \sum_{\ell=2}^j (-1)^\ell \Pi_{j,j}^\ell + \sum_{\ell=1}^j (-1)^\ell \sum_{k_1=1}^{j-1} \Pi_{j,k_1}^\ell \right). \end{aligned}$$

Using the recurrence relation given by Lemma 6.4 and a change of indices lead to

$$\begin{aligned} \rho^{(j)} &= \rho^n + \Delta t \nabla_x \cdot \left(-\Pi_{j,j}^1 + \sum_{\ell=2}^j (-1)^\ell \sum_{k_1=1}^{j-1} \Pi_{j,k_1}^{\ell-1} + \sum_{\ell=1}^j (-1)^\ell \sum_{k_1=1}^{j-1} \Pi_{j,k_1}^\ell \right) \\ &= \rho^n + \Delta t \nabla_x \cdot \left(-\Pi_{j,j}^1 - \sum_{\ell=1}^{j-1} (-1)^\ell \sum_{k_1=1}^{j-1} \Pi_{j,k_1}^\ell + \sum_{\ell=1}^j (-1)^\ell \sum_{k_1=1}^{j-1} \Pi_{j,k_1}^\ell \right) \\ &= \rho^n + \Delta t \nabla_x \cdot \left(-\Pi_{j,j}^1 + (-1)^j \sum_{k_1=1}^{j-1} \Pi_{j,k_1}^j \right). \end{aligned}$$

From Lemma 6.4, we have $\sum_{k_1=1}^{j-1} \Pi_{j,k_1}^j = 0$, so that from Definition 6.3 we get

$$\begin{aligned} \rho^{(j)} &= \rho^n + \Delta t \nabla_x \cdot \left(-\Pi_{j,j}^1 \right) = \rho^n - \Delta t \nabla_x \cdot \left(\left\langle v \frac{a_{jj}}{a_{jj}} \mathcal{S}^{k_0} \mathcal{R}^{k_1=j} \right\rangle_V \right) \\ &= \rho^n - \Delta t \nabla_x \cdot \left(\left\langle v \left(\sum_{k_2=1}^{k_1} a_{k_1 k_2} L^{-1}(vM) \cdot \nabla_x \rho^{(k_2)} - \sum_{k_2=1}^{k_1-1} \tilde{a}_{k_1 k_2} L^{-1}(vM) \cdot A \rho^{(k_2)} \right) \right\rangle_V \right)_{k_1=j} \\ &= \rho^n - \Delta t \sum_{k_2=1}^j a_{jk_2} \nabla_x \cdot \left(\langle v \otimes L^{-1}(vM) \rangle_V \nabla_x \rho^{(k_2)} \right) + \Delta t \sum_{k_2=1}^{j-1} \tilde{a}_{jk_2} \nabla_x \cdot \left(\langle v \otimes L^{-1}(vM) \rangle_V A \rho^{(k_2)} \right), \end{aligned}$$

which ends the proof.

□

Remark 6.7. For CK-ARS schemes with well-prepared initial data, we obtain $g^{(1)} = g^n = O(\epsilon)$ and $\rho^{(1)} = \rho^n$. The presentation in this section will apply for CK-ARS from the second RK stage onwards. For instance, Definition 6.3 applies for CK-ARS with the following change in indexes: $j \in \{2, 3, \dots, s\}$, $k_1, m \in \{2, 3, \dots, j\}$ and all the summations involved start from 2 instead of 1 since $a_{11} = 0$. The lemmas and theorems that follow also undergo the corresponding change in indexes, and the AP property for CK-ARS can be observed for $j \in \{2, 3, \dots, s\}$.

Remark 6.8. Upon incorporating the spatial matrices corresponding to staggered grid in place of the continuous gradient operator, we obtain in the limit $\epsilon \rightarrow 0$,

$$\begin{aligned} \rho^{(j)} &= (I + a_{jj} \Delta t \mathbf{G}_{\text{cen}_\rho} (\langle v \otimes L^{-1}(vM) \rangle_V \mathbf{G}_{\text{cen}_g}))^{-1} \\ &\times \left(\rho^n - \sum_{k=1}^{j-1} a_{jk} \Delta t \mathbf{G}_{\text{cen}_\rho} (\langle v \otimes L^{-1}(vM) \rangle_V \mathbf{G}_{\text{cen}_g} \rho^{(k)}) \right. \\ &\left. + \sum_{k=1}^{j-1} \tilde{a}_{jk} \Delta t \mathbf{G}_{\text{cen}_\rho} (\langle v \otimes L^{-1}(vM) \rangle_V \mathbf{G}_{\text{avg}_g} A \rho^{(k)}) \right). \end{aligned} \tag{6.13}$$

The matrices $\mathbf{G}_{\text{cen}_\rho}$, $\mathbf{G}_{\text{cen}_g}$ are given in Section 5.2 and $\mathbf{G}_{\text{avg}_g} = \frac{1}{2} \text{circ}([1, 1])$. Thus, $(\mathbf{G}_{\text{avg}_g} A(\rho^{(k)}))_{i+1/2} = \frac{1}{2} A(\rho_{i+1}^{(k)} + \rho_i^{(k)})$. This results in a central discretization of the advection term in the macro equation. Thus, we obtain a consistent internal RK stage approximation of the advection-diffusion equation in the limit $\epsilon \rightarrow 0$.

To obtain an upwind discretization of the advection term, we use the space operator \mathbf{G}_{up_g} on $A\rho^{(k)}$ instead of $\mathbf{G}_{\text{avg}_g}$. This is defined as follows:

$$\left(\mathbf{G}_{\text{up}_g} A(\rho^{(k)}) \right)_{i+1/2} = \begin{cases} A\rho_i^{(k)} & \text{if } A \geq 0 \\ A\rho_{i+1}^{(k)} & \text{if } A < 0. \end{cases} \tag{6.14}$$

This results in a first order upwind discretization of the advection term. For second order upwind discretization, the following is required:

$$\left(\mathbf{G}_{\text{up}_g} A(\rho^{(k)}) \right)_{i+1/2} = \begin{cases} A\left(\frac{3}{2}\rho_i^{(k)} - \frac{1}{2}\rho_{i-1}^{(k)}\right) & \text{if } A \geq 0 \\ A\left(\frac{3}{2}\rho_{i+1}^{(k)} - \frac{1}{2}\rho_{i+2}^{(k)}\right) & \text{if } A < 0. \end{cases} \tag{6.15}$$

6.2. Inflow boundaries

So far, periodic boundary conditions were considered. In this part, we consider inflow boundary conditions for f which is solution to (2.1)

$$f(t, x, v) = f_b(t, x, v), \quad (x, v) \in \partial\Omega \times V \text{ such that } v \cdot n(x) < 0, \quad \forall t, \tag{6.16}$$

where f_b is a given function and $n(x)$ denotes the unitary outgoing normal vector to $\partial\Omega$. As mentioned in [29, 30], such boundary conditions cannot be adapted naturally to the standard micro-macro unknowns $\rho(t, x)$ and $g(t, x, v)$ which form a solution to (2.6) and a specific treatment with artificial boundary conditions is required (see [29, 30, 33]). To overcome this drawback, another micro-macro decomposition is introduced in [29]

$$f = \bar{\rho}M + \bar{g}, \quad \bar{\rho}(t, x) = \langle f(t, x, \cdot) \rangle_{V_-}, \quad \langle \bar{g}(t, x, \cdot) \rangle_{V_-} = 0, \quad \langle f \rangle_{V_-} = \frac{\int_{V_-} f \, d\mu}{\int_{V_-} M \, d\mu}, \tag{6.17}$$

where the velocity domain V_- is defined by

$$V_-(x) = \{v \in V, \omega(x, v) < 0\}, \quad V_+(x) = V \setminus V_-(x). \tag{6.18}$$

The function $\omega(x, v)$ extends $v \cdot n(x)$ in the interior of domain. Some examples of $\omega(x, v)$ for different geometries are provided in [29]. It can be seen that the boundary conditions for $\bar{\rho}(t, x)$ and $\bar{g}(t, x, v)$ can be evaluated from the inflow boundary condition in equation (6.16). Indeed, for $(x, v) \in \partial\Omega \times V$ such that $v \cdot n(x) < 0, \forall t$, we define

$$\bar{\rho}_b(t, x) = \langle f_b(t, x, \cdot) \rangle_{V_-}, \quad \bar{g}_b(t, x, v) = f_b(t, x, v) - \bar{\rho}_b(t, x)M(v). \tag{6.19}$$

The derivation of the micro-macro model needs to be adapted to this decomposition. The projector Π^- is defined as $\Pi^-h = \langle h \rangle_{V_-}M$. Then, substituting equation (6.17) into equation (2.1) and applying Π^- and $I - \Pi^-$ enable to get the macro and micro equations:

$$\partial_t \bar{\rho} + \frac{1}{\epsilon} \langle vM \rangle_{V_-} \cdot \nabla_x \bar{\rho} + \frac{1}{\epsilon} \nabla_x \cdot \langle v\bar{g} \rangle_{V_-} = \frac{1}{\epsilon^2} \langle L\bar{g} \rangle_{V_-}, \tag{6.20}$$

$$\partial_t \bar{g} + \frac{1}{\epsilon} (I - \Pi^-)(v \cdot \nabla_x \bar{g}) + \frac{1}{\epsilon} (I - \Pi^-)vM \cdot \nabla_x \bar{\rho} = \frac{1}{\epsilon^2} \tilde{L}\bar{g}, \tag{6.21}$$

where $\tilde{L} = (I - \Pi^-)L$. Moreover, it can be seen that $\tilde{L} = (I - \Pi^-)L(I - \Pi^-) = (I - \Pi^-)L(I - \Pi)$ since $\Pi^-h, \Pi h \in \mathcal{N}(L), \forall h$.

The macro equation (6.20) turns out to be more complicated than the one obtained for standard micro-macro decomposition. It can be made simpler by using $\rho = \bar{\rho} + \langle \bar{g} \rangle_V, f = \rho M - \langle \bar{g} \rangle_V M + \bar{g}$, obtained from the decompositions (2.6) and (6.17). Applying Π to equation (2.1) instead of Π^- , we obtain the simpler macro equation,

$$\partial_t \rho + \frac{1}{\epsilon} \nabla_x \cdot \langle v\bar{g} \rangle_V = 0, \tag{6.22}$$

and the micro-macro system that we will consider in the sequel is (6.21) and (6.22).

6.2.1. Numerical scheme

In this part, we present the fully discretized scheme to approximate (6.21) and (6.22). The boundary conditions on $\bar{\rho}_b$ and \bar{g}_b in equation (6.19) will be utilised along with the relation $\rho = \bar{\rho} + \langle \bar{g} \rangle_V$ that allows to link ρ and $\bar{\rho}$ in the interior of the domain. We will use a staggered grid in space following [29] and a high order scheme in time, following the strategy developed previously. To ease the reading, only the first order version will be presented.

We present the space approximation based on a staggered grid. Let us consider the space interval $[0, L]$ with two grids: $x_i = i\Delta x$ and $x_{i+1/2} = (i + 1/2)\Delta x, \Delta x = L/(N_x - 1)$. The ‘interior’ variables such as $\rho, \bar{\rho}$ are stored at grid points x_i with $i = 1, \dots, N_x - 2$ and \bar{g} is stored at $i + 1/2 = 1/2, \dots, N_x - 3/2$. We also use the variable $\bar{g}_{cl} = \bar{g} \cup \bar{g}_b \in \mathbb{R}^{N_x+1}$. The whole domain including boundary will be considered for the micro unknown \bar{g} so that the components of \bar{g}_{cl} correspond to the grid indices $i + 1/2 = -1/2, \dots, N_x - 1/2$. The matrices corresponding to spatial operators are given by

$$\mathbf{B}_{\text{upw}}^- = \frac{1}{\Delta x} \text{circ}([-1, 1])_{(N_x-1) \times (N_x+1)}, \quad \mathbf{B}_{\text{upw}}^+ = \frac{1}{\Delta x} \text{circ}([0, -1, 1])_{(N_x-1) \times (N_x+1)}, \tag{6.23}$$

$$\mathbf{B}_{\text{cen}_\rho} = \frac{1}{\Delta x} \text{circ}([-1, 1])_{(N_x-2) \times (N_x-1)}, \quad \mathbf{B}_{\text{avg}} = \frac{1}{2} \text{circ}([1, 1])_{(N_x-2) \times (N_x-1)}, \tag{6.24}$$

$$\mathbf{B}_{\text{cen}_g} = \frac{1}{\Delta x} \text{circ}_b([-1, 1])_{(N_x-1) \times (N_x-2)}. \tag{6.25}$$

The circ_b definition is presented in Appendix A. Further, we also introduce a vector containing the boundary values of $\bar{\rho}$ as $\bar{\rho}_{bd} = \frac{1}{\Delta x} [-\bar{\rho}_{b_{i=0}}, 0, 0, \dots, 0, \bar{\rho}_{b_{i=N_x-1}}]_{(N_x-1) \times 1}^T$. We now present our scheme by using this matrix notation. For simplicity, we assume that $\bar{\rho}_{bd}$ is time invariant. We also use the following notations:

$$\bar{\mathcal{T}}h = (I - \Pi^-)(v^+ \mathbf{B}_{\text{upw}}^- + v^- \mathbf{B}_{\text{upw}}^+)h, \quad \bar{\mathcal{D}}_{\epsilon, \Delta t} = \left\langle v \left(\epsilon^2 I - \Delta t \tilde{L} \right)^{-1} \Delta t (I - \Pi^-)(vM) \right\rangle_V,$$

$$\bar{\mathcal{E}}_{\epsilon, \Delta t} = \left\langle \left(\epsilon^2 I - \Delta t \tilde{L} \right)^{-1} \Delta t (I - \Pi^-) (vM) \right\rangle_V, \quad \bar{\mathcal{I}}_{\epsilon, \Delta t} = \left(\epsilon^2 I - \Delta t \tilde{L} \right)^{-1}, \quad \bar{\mathcal{J}} = (I - \Pi^-) (vM).$$

The micro equation (6.21) is discretised in time as in the previous (periodic) case

$$\bar{g}^{n+1} = \bar{\mathcal{I}}_{\epsilon, \Delta t} \left(\epsilon^2 \bar{g}^n - \epsilon \Delta t \bar{\mathcal{T}} \bar{g}_{cl}^n - \epsilon \Delta t \bar{\mathcal{J}} \mathbf{B}_{\text{cen}_g} \bar{\rho}^{n+1} - \epsilon \Delta t \bar{\mathcal{J}} \bar{\rho}_{bd} \right), \tag{6.26}$$

and for the macro equation (6.22), we obtain

$$\frac{\rho^{n+1} - \rho^n}{\Delta t} + \frac{1}{\epsilon} \langle v \mathbf{B}_{\text{cen}_\rho} \bar{g}^{n+1} \rangle_V = 0.$$

Substituting \bar{g}^{n+1} in the above equation, we get

$$\rho^{n+1} = \rho^n - \Delta t \mathbf{B}_{\text{cen}_\rho} \langle v \bar{\mathcal{I}}_{\epsilon, \Delta t} (\epsilon \bar{g}^n - \Delta t \bar{\mathcal{T}} \bar{g}_{cl}^n - \Delta t \bar{\mathcal{J}} \mathbf{B}_{\text{cen}_g} \bar{\rho}^{n+1} - \Delta t \bar{\mathcal{J}} \bar{\rho}_{bd}) \rangle_V. \tag{6.27}$$

In index notation, we use $\rho_i^{n+1} = \bar{\rho}_i^{n+1} + \frac{1}{2} \langle \bar{g}_{i-1/2}^{n+1} + \bar{g}_{i+1/2}^{n+1} \rangle_V$ (since $\rho = \bar{\rho} + \langle \bar{g} \rangle_V$) to match the two grids. In matrix notation, this becomes $\rho^{n+1} = \bar{\rho}^{n+1} + \mathbf{B}_{\text{avg}} \langle \bar{g}^{n+1} \rangle_V$ with \mathbf{B}_{avg} given by (6.24). Substituting this into the above equation and inserting the expression for \bar{g}^{n+1} into $\mathbf{B}_{\text{avg}} \langle \bar{g}^{n+1} \rangle_V$ enable to update the interior macro unknown

$$\begin{aligned} \bar{\rho}^{n+1} &= \left(I - \epsilon \mathbf{B}_{\text{avg}} (\bar{\mathcal{E}}_{\epsilon, \Delta t} \mathbf{B}_{\text{cen}_g}) - \Delta t \mathbf{B}_{\text{cen}_\rho} (\bar{\mathcal{D}}_{\epsilon, \Delta t} \mathbf{B}_{\text{cen}_g}) \right)^{-1} \\ &\quad \times \left(\rho^n - \mathbf{B}_{\text{avg}} \langle \bar{\mathcal{I}}_{\epsilon, \Delta t} (\epsilon^2 \bar{g}^n - \epsilon \Delta t \bar{\mathcal{T}} \bar{g}_{cl}^n - \epsilon \Delta t \bar{\mathcal{J}} \bar{\rho}_{bd}) \rangle_V \right. \\ &\quad \left. - \Delta t \mathbf{B}_{\text{cen}_\rho} \langle v \bar{\mathcal{I}}_{\epsilon, \Delta t} (\epsilon \bar{g}^n - \Delta t \bar{\mathcal{T}} \bar{g}_{cl}^n - \Delta t \bar{\mathcal{J}} \bar{\rho}_{bd}) \rangle_V \right). \end{aligned} \tag{6.28}$$

The right hand side of above expression involves only known quantities so that $\bar{\rho}^{n+1}$ can be updated from (6.28) which can then be used to update \bar{g}^{n+1} in (6.26). Then, we update \bar{g}_{cl}^{n+1} thanks to the boundary conditions (6.19), and finally ρ^{n+1} can be computed from $\rho^{n+1} = \bar{\rho}^{n+1} + \mathbf{B}_{\text{avg}} \langle \bar{g}^{n+1} \rangle_V$. In the limit $\epsilon \rightarrow 0$, the above equation becomes,

$$\bar{\rho}^{n+1} = \left(I + \Delta t \mathbf{B}_{\text{cen}_\rho} \left(\langle v \otimes \tilde{L}^{-1} \bar{\mathcal{J}} \rangle_V \mathbf{B}_{\text{cen}_g} \right) \right)^{-1} \left(\rho^n - \Delta t \mathbf{B}_{\text{cen}_\rho} \left(\langle v \otimes \tilde{L}^{-1} \bar{\mathcal{J}} \rangle_V \bar{\rho}_{bd} \right) \right).$$

This is a consistent discretization of the diffusion equation in equation (2.5) since $\langle v \otimes \tilde{L}^{-1} \bar{\mathcal{J}} \rangle_V = \langle v \otimes L^{-1} (vM) \rangle_V = -\kappa$. Further, the high order scheme in time can be constructed in a similar manner as before.

We now present the evaluation of boundary condition on ρ . For $i = 1/2$ and $i = 3/2$, the micro equation in (6.26) simplifies as:

$$\bar{g}_{\frac{1}{2}}^{n+1} = \left(-\Delta t \tilde{L} \right)^{-1} \left(-\epsilon \Delta t (I - \Pi^-) vM \frac{\bar{\rho}_1^{n+1} - \bar{\rho}_0^{n+1}}{\Delta x} + 2\epsilon \Delta t (I - \Pi^-) v^+ \frac{\bar{g}_0^n}{\Delta x} \right) + \mathcal{O}(\epsilon^2) \tag{6.29}$$

$$\bar{g}_{\frac{3}{2}}^{n+1} = \left(-\Delta t \tilde{L} \right)^{-1} \left(-\epsilon \Delta t (I - \Pi^-) vM \frac{\bar{\rho}_2^{n+1} - \bar{\rho}_1^{n+1}}{\Delta x} \right) + \mathcal{O}(\epsilon^2) \tag{6.30}$$

since $\bar{g}_{-\frac{1}{2}}^n = 2\bar{g}_0^n - \bar{g}_{\frac{1}{2}}^n$, and $\bar{g}_{i+\frac{1}{2}}^n = \mathcal{O}(\epsilon)$ for all $n \geq 1$ and $i + \frac{1}{2} = 1/2, 3/2, 5/2$. Inserting these into the macro equation corresponding to $i = 1$ and simplifying, we obtain

$$\rho_1^{n+1} = \rho_1^n - \frac{\Delta t}{\epsilon} \left\langle v \frac{\bar{g}_{\frac{3}{2}}^{n+1} - \bar{g}_{\frac{1}{2}}^{n+1}}{\Delta x} \right\rangle_V \tag{6.31}$$

$$= \rho_1^n - \frac{\Delta t}{\Delta x^2} \left\langle v \tilde{L}^{-1} (I - \Pi^-) (vM) \right\rangle_V (\bar{\rho}_2^{n+1} - 2\bar{\rho}_1^{n+1} + \bar{\rho}_0^{n+1}) - \frac{\Delta t}{\Delta x^2} 2 \left\langle v \tilde{L}^{-1} (I - \Pi^-) (v^+ \bar{g}_0^n) \right\rangle_V \tag{6.32}$$

up to $\mathcal{O}(\epsilon)$. Further, observing that $\langle v\tilde{L}^{-1}(I - \Pi^-)(vM) \rangle = \langle vL^{-1}(vM) \rangle_V$ and $\langle v\tilde{L}^{-1}(I - \Pi^-)(v^+\bar{g}_0^n) \rangle_V = \langle vL^{-1}(I - \Pi)(v^+\bar{g}_0^n) \rangle_V$, and inserting $\bar{g}_0^n = f_0^n - \bar{\rho}_0^n M$ into the above equation lead to:

$$\begin{aligned} \rho_1^{n+1} &= \rho_1^n - \frac{\Delta t}{\Delta x^2} \langle vL^{-1}(vM) \rangle_V \\ &\times \left(\bar{\rho}_2^{n+1} - 2\bar{\rho}_1^{n+1} + \bar{\rho}_0^{n+1} - 2 \frac{\langle vL^{-1}(I - \Pi)(v^+M) \rangle_V}{\langle vL^{-1}(vM) \rangle_V} \bar{\rho}_0^n + 2 \frac{\langle vL^{-1}(I - \Pi)(v^+f_0^n) \rangle_V}{\langle vL^{-1}(vM) \rangle_V} \right). \end{aligned} \quad (6.33)$$

For both choices $M(v) = 1$ on $V = [-1, 1]$ and $M(v) = \frac{1}{\sqrt{2\pi}}e^{-v^2/2}$ on $V = \mathbb{R}$, we observe that $2 \frac{\langle vL^{-1}(I - \Pi)(v^+M) \rangle_V}{\langle vL^{-1}(vM) \rangle_V} = 1$. Hence, for these cases with constant in time boundary conditions, the above equation simplifies as:

$$\rho_1^{n+1} = \rho_1^n - \frac{\Delta t}{\Delta x^2} \langle vL^{-1}(vM) \rangle_V \left(\bar{\rho}_2^{n+1} - 2\bar{\rho}_1^{n+1} + 2 \frac{\langle vL^{-1}(I - \Pi)(v^+f_0^n) \rangle_V}{\langle vL^{-1}(vM) \rangle_V} \right) \quad (6.34)$$

where $\bar{\rho}_0 = 2 \frac{\langle vL^{-1}(I - \Pi)(v^+f_0^n) \rangle_V}{\langle vL^{-1}(vM) \rangle_V}$ is the boundary value of the micro-macro numerical scheme in the diffusion limit. For $M(v) = \frac{1}{\sqrt{2\pi}}e^{-v^2/2}$ on $V = \mathbb{R}$, this evaluates to $\bar{\rho}_0 = 2\sqrt{\frac{2}{\pi}} \simeq 1.59$. In the work by [29], this value is evaluated to be $\bar{\rho}_0 = 0.75$ for $M(v) = 1$ on $V = [-1, 1]$.

7. NUMERICAL RESULTS

In this section, we present the numerical validation of our high order asymptotic preserving schemes in different configurations.

7.1. Diffusion asymptotics

First, we check time and space accuracy for the micro-macro scheme in the diffusion limit.

7.1.1. Time order of accuracy

The spatial domain $L = [0, 2\pi]$ of the problem is discretized using $N_x = 50$ grid points. The velocity domain is truncated to $[-v_{\max}, v_{\max}]$ with $v_{\max} = 5$ and we take $\Delta v = 1$. The initial condition is:

$$\rho(0, x) = 1 + \cos(x)$$

$$\text{Well-prepared data (WP): } g(0, x, v) = \epsilon^2(I - \Pi)(v^2M)\rho(0, x)$$

$$\text{Non-well-prepared data (N-WP): } g(0, x, v) = (I - \Pi)(v^2M)\rho(0, x),$$

with $M(v) = \frac{1}{\sqrt{2\pi}}e^{-v^2/2}$. Periodic boundary conditions are used on both ρ and g . The spatial terms are discretised by using the atmost-third order accurate matrices on non-staggered grid presented in Section 5.3. The final time is $T = 0.5$, and the following Δt are considered to validate the different high order time integrators: $\Delta t = 0.5, 0.1, 0.05, 0.01, 0.005, 0.001$. The type A micro-macro schemes constructed using the Butcher tableau corresponding to DP-A(1, 2, 1), DP2-A(2, 4, 2) and DP1-A(2, 4, 2) are considered. Although DP1-A(2, 4, 2) is second order accurate, the implicit part of it when used separately is third order accurate. Further, we also consider the type CK-ARS micro-macro schemes constructed using Butcher tableau corresponding to ARS(1, 1, 1), ARS(2, 2, 2) and ARS(4, 4, 3). The Butcher tableau of different time integrators utilised are presented in Appendix B.

In Figure 1, we plot the time error for the different time integrators in both WP and N-WP cases and for different values of ϵ . Note that the reference solution for each curve is obtained by using the same micro-macro scheme corresponding to that curve with $\Delta t = 10^{-4}$. For $\epsilon = 1$, the required orders of accuracy are recovered for

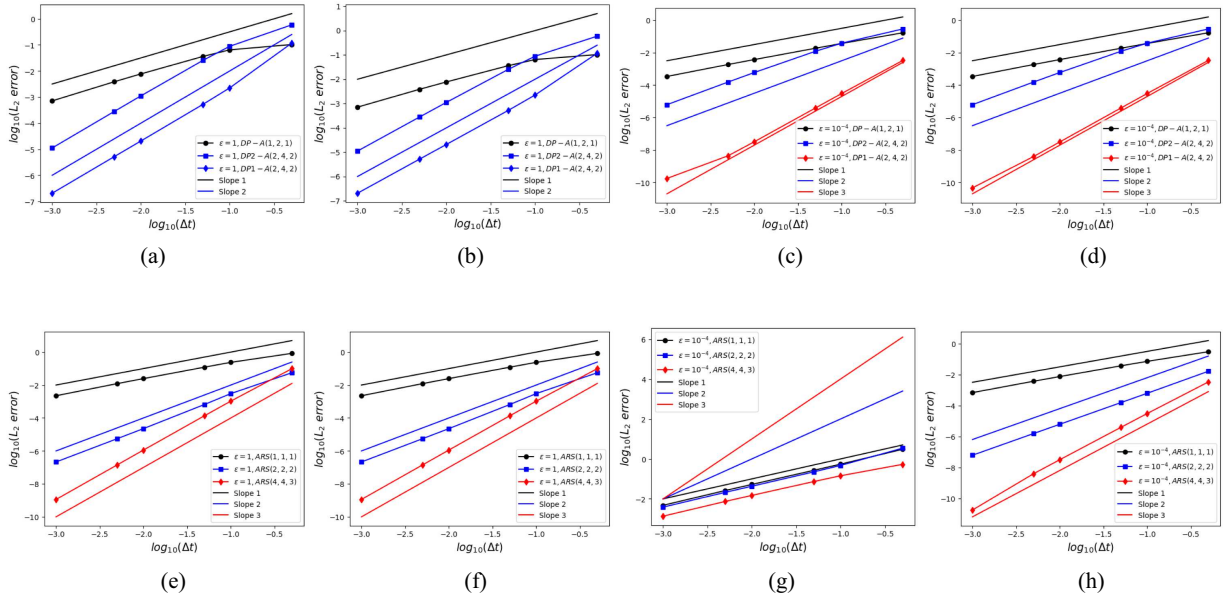


FIGURE 1. Accuracy in time for different type A and CK-ARS time integrators (both WP and N-WP initial data). The reference solution is obtained from the micro-macro with $\Delta t = 10^{-4}$. (a) A N-WP, $\epsilon = 1$. (b) A WP, $\epsilon = 1$. (c) A N-WP, $\epsilon = 10^{-4}$. (d) A WP, $\epsilon = 10^{-4}$. (e) CK N-WP, $\epsilon = 1$. (f) CK WP, $\epsilon = 1$. (g) CK N-WP, $\epsilon = 10^{-4}$. (h) CK WP, $\epsilon = 10^{-4}$.

type A schemes with both N-WP and WP initial data, as observed in Figures 1a and 1b. For $\epsilon = 10^{-4}$, due to the asymptotic degeneracy of our scheme into a fully-implicit scheme for diffusion equation, only the implicit part of the Butcher tableau plays a role. Hence DP1-A(2, 4, 2) becomes third order accurate in time, while DP-A(1, 2, 1) and DP2-A(2, 4, 2) are first and second order accurate respectively. This is shown in Figures 1c and 1d. On the other hand, CK-ARS schemes with both N-WP and WP initial data for $\epsilon = 1$ recover the required orders of accuracy as shown in Figures 1e and 1f. However, for $\epsilon = 10^{-4}$, required orders of accuracy are observed only when WP initial data are used (Fig. 1h). As shown in the analyses presented in previous sections, usage of N-WP initial data for CK-ARS time integrators does not allow the asymptotic accuracy (Fig. 1g). The required order of accuracy for N-WP initial data with CK-ARS time integrator can be obtained by modifying the initial few time steps as Δt^p for p th order accurate scheme as discussed in [33, 35]. On the other hand, the type A time integrators DP1-A(2, 4, 2) and DP2-A(2, 4, 2) that we have used do not require such initial time step reduction for maintaining the required order of accuracy.

Since we proved the asymptotic preserving property, the diffusion solution is used as reference solution in the asymptotic regime ($\epsilon = 10^{-4}$) with $\Delta t = 10^{-4}$ (in Fig. 2) to check the orders of accuracy of high order integrators. The results are similar to the ones obtained for $\epsilon = 10^{-4}$ in Figure 1, except that here we observe a plateau for third order scheme and small Δt . This is due to the $\mathcal{O}(\epsilon^2)$ difference between the schemes based on micro-macro and diffusion models. This error dominates $\mathcal{O}(\Delta t^3)$ error, and hence it is observed.

7.1.2. Space order of accuracy

The problem set-up is the same as described in the previous subsection, except for the following changes. Here, we consider the final time to be $T = 0.01$ and $\Delta t = 0.001$ so that the error in time is small enough to study the spatial accuracy. To do so, we consider the following number of points in space: $N_x = 20, 24, 30, 40$ and 60. The reference solution is obtained with $N_x = 120$.

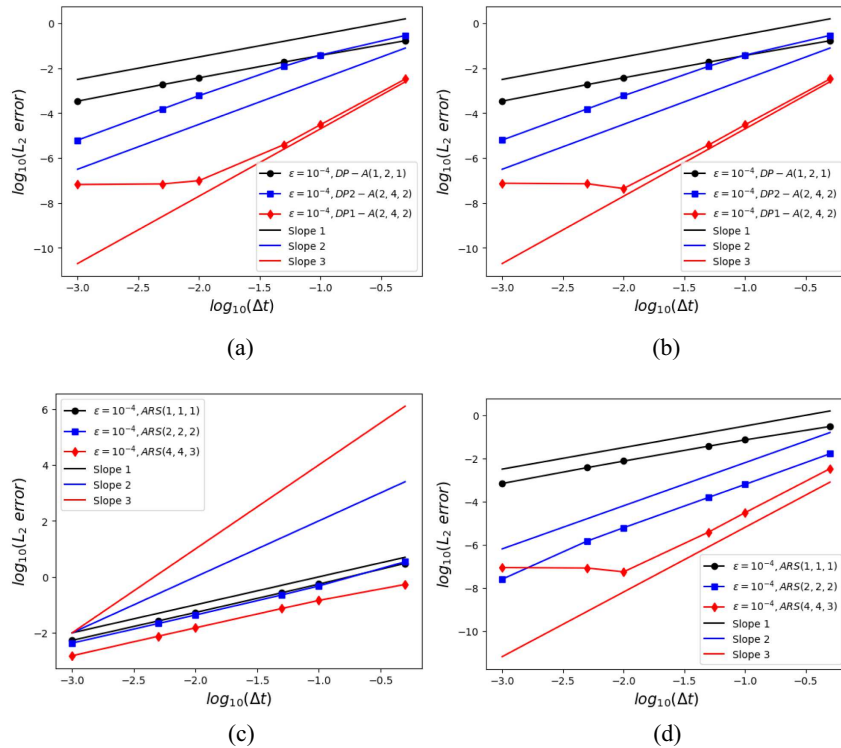


FIGURE 2. Accuracy in time for different type A and CK-ARS time integrators (both WP and N-WP initial data). The reference solution is obtained from the diffusion equation with $\Delta t = 10^{-4}$. (a) A N-WP. (b) A WP. (c) CK N-WP. (d) CK WP.

Since the spatial accuracy plots obtained from different time integrators are quite similar, we present only the plots obtained by using DP1-A(2, 4, 2) and ARS(4, 4, 3) for different values of ϵ ($\epsilon = 10^{-4}, 0.2, 1$) in Figures 3a and 3b. For the spatial discretization, we only show the results obtained by the third order spatial matrices on non-staggered grid presented in Section 5.3 so that the scheme is expected to be third order accurate in space. In Figures 3a and 3b, the expected order is observed for the two time integrators and for the three considered values of ϵ .

7.1.3. Qualitative results

In this part, we compare the density obtained by the micro-macro equation (MM), the linear kinetic equation with BGK collision operator (BGK) and the asymptotic diffusion equation, for different values of ϵ . The MM scheme described in previous sections is utilised, the BGK is discretized using an IMEX (implicit treatment of collision term and explicit treatment of transport term) scheme whereas for the diffusion model, an implicit scheme is used. For all three models, the Butcher tableau corresponding to DP1-A(2, 4, 2) time integrator is used. For the spatial discretization, we use third order scheme on non-staggered grid.

The problem domain $L = [0, 2\pi]$ is discretised using $N_x = 20$ grid points for all the three models. The final time is $T = 0.5$, and $\Delta t = 0.005$. We use the same N-WP initial and boundary conditions described in the previous subsection. Further, we also consider the same velocity discretization as before for both MM and BGK models.

In Figure 4a for rarefied regime ($\epsilon = 1$), the MM and BGK models compare very well, while the diffusion model is different as expected. In the intermediate regime ($\epsilon = 0.2$), the BGK and MM models match very well

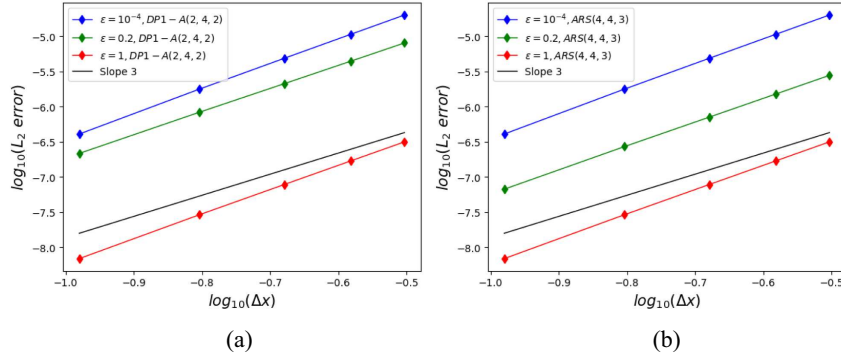


FIGURE 3. Accuracy in space for the third order spatial scheme coupled with different time approximations. (a) DP1-A(2, 4, 2) type A with N-WP initial data. (b) ARS(4, 4, 3) type CK-ARS with WP initial data.

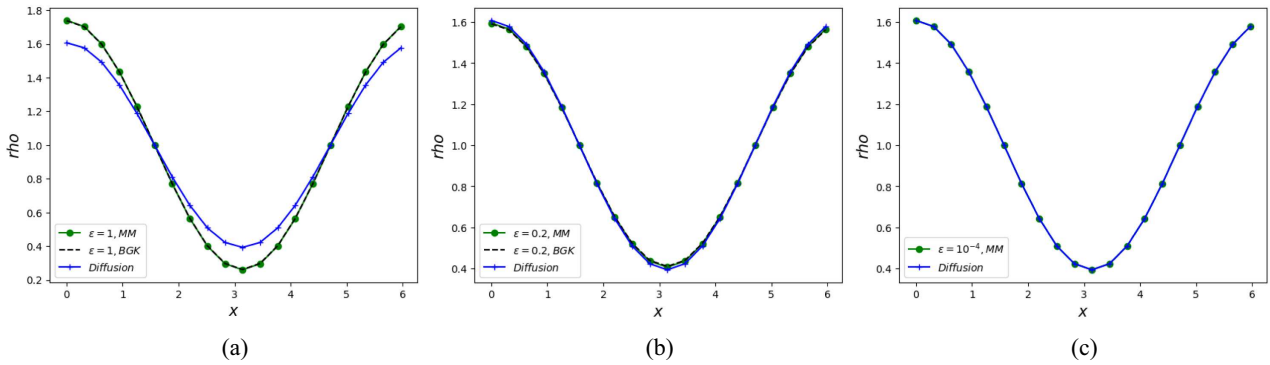


FIGURE 4. Qualitative results for diffusion asymptotics. (a) $\epsilon = 1$. (b) $\epsilon = 0.4$. (c) $\epsilon = 10^{-4}$.

while the diffusion model is slightly different. For $\epsilon = 10^{-4}$, we only compare MM and the diffusion in Figure 4c and illustrate the AP property of the time integrators used for MM.

7.2. Advection-diffusion asymptotics

In this subsection, we present the time accuracy of our high order micro-macro scheme for the advection-diffusion case. As in the diffusion case, the spatial domain $L = [0, 2\pi]$ is discretised using $N_x = 20$ grid points whereas the velocity domain is $[-v_{\max}, v_{\max}]$ with $v_{\max} = 5$ and $\Delta v = 1$. The initial condition for the problem is:

$$\rho(0, x) = \sin(x) \tag{7.1}$$

$$\text{Well-prepared data (WP): } g(0, x, v) = \epsilon^2(I - \Pi)(v^2 M)\rho(0, x) \tag{7.2}$$

$$\text{Non-well-prepared data (N-WP): } g(0, x, v) = (I - \Pi)(v^2 M)\rho(0, x), \tag{7.3}$$

with $M(v) = \frac{1}{\sqrt{2\pi}}e^{-v^2/2}$. Periodic boundary conditions are used on both ρ and g . The spatial terms are discretised by using the atmost-first order accurate matrices on staggered grid presented in Section 5.2. The final time is $T = 0.5$, and the following time steps are considered: $\Delta t = 0.5, 0.1, 0.05, 0.01, 0.005, 0.001$. We observe the time order of accuracy for both $\epsilon = 1$ and $\epsilon = 10^{-4}$. We choose the highest order time integrator in both type A and CK-ARS schemes for studying the time accuracy. Hence, we consider DP1-A(2, 4, 2) and ARS(4, 4, 3) with N-WP and WP data respectively.

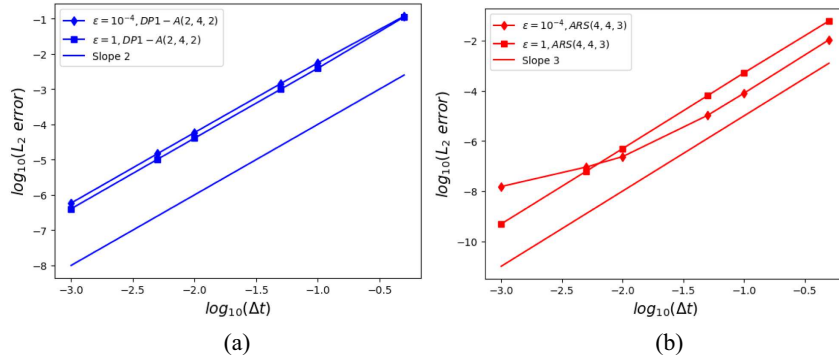


FIGURE 5. Accuracy in time. (a) DP1-A(2, 4, 2) type A with N-WP initial data. (b) ARS(4, 4, 3) type CK-ARS with WP initial data. The reference solution is obtained from the micro-macro scheme with $\Delta t = 10^{-4}$.

Asymptotically, our micro-macro scheme degenerates to a consistent scheme for the advection-diffusion equation with advection and diffusion terms being treated explicitly and implicitly respectively. Hence, unlike the case of diffusion asymptotics for which an extra order is observed asymptotically, DP1-A(2, 4, 2) remains second order accurate for $\epsilon = 10^{-4}$ since both explicit and implicit matrices of the Butcher tableau are involved here (Fig. 5a). For $\epsilon = 1$, the required second order accuracy is observed. Further, the required third order accuracy of ARS(4, 4, 3) is observed for both $\epsilon = 10^{-4}$, 1 in Figure 5b, since well-prepared initial data is considered.

7.3. Inflow boundary condition

In this subsection, the high order numerical scheme for micro-macro model that allows inflow boundary conditions is validated numerically. We first present the time accuracy results for high order schemes. Then, some qualitative plots are shown for two tests with zero inflow at the right boundary, and equilibrium and non-equilibrium inflows respectively at the left boundary.

7.3.1. Time order of accuracy

If the domain of the problem is a half-plane, $\omega(x, v) = [-v, 0, 0, \dots]$ can be chosen $\forall x$ as described in [29]. Here, for numerical purposes, we consider a domain of $L = [0, 2]$ and assume that the right boundary does not influence the dynamics.

The spatial domain is discretised using $N_x = 20$ grid points and the velocity domain is $[-v_{\max}, v_{\max}]$ with $v_{\max} = 5$ and $\Delta v = 1$. The initial conditions at all interior points and right boundary conditions for the variables ρ , $\bar{\rho}$ and \bar{g} are considered to be 0. The left boundary conditions (for $v_k > 0$) are:

$$f(t, x_i = 0, v_k) = M(v_k), \quad \bar{\rho}(t, x_i = 0) = 1, \quad \bar{g}(t, x_{i+1/2} = -\Delta x/2, v_k) = 0, \quad (7.4)$$

with $M(v) = \frac{1}{\sqrt{2\pi}} e^{-v^2/2}$. The final time is $T = 0.1$, and the following time steps are considered to check the accuracy in time: $\Delta t = 0.1, 0.05, 0.01, 0.005, 0.001$. Like in the previous problems, we observe the time order of accuracy for both $\epsilon = 1$ and $\epsilon = 10^{-4}$. The time integrators considered are DP-A(1, 2, 1) and DP1-A(2, 4, 2). The reference solution for each curve in Figure 6 is obtained by using the same micro-macro scheme corresponding to that curve with $\Delta t = 10^{-4}$. For type A time integrators with $\epsilon = 1$ in Figure 6a, first and second order accuracies of DP-A(1, 2, 1) and DP1-A(2, 4, 2) are observed. In Figure 6b for $\epsilon = 10^{-4}$, first and third order accuracies of DP-A(1, 2, 1) and DP1-A(2, 4, 2) respectively are observed. As for the (periodic) diffusion case, DP1-A(2, 4, 2) turns out to be third order accurate since only the implicit part of Butcher tableau is involved asymptotically. For ARS(2, 2, 2) and ARS(4, 4, 3) time integrators (not shown here), order reduction to first

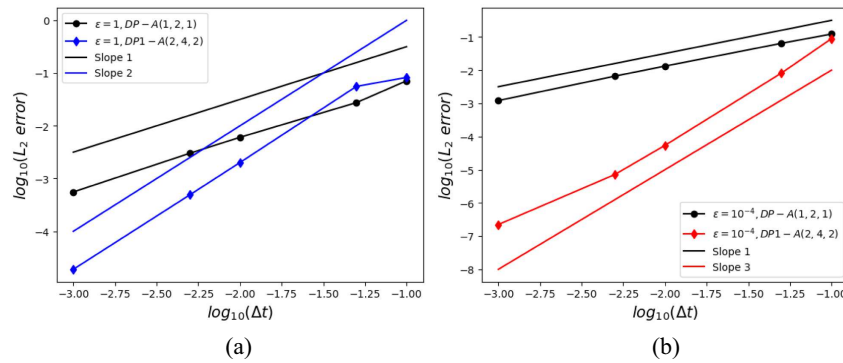


FIGURE 6. Accuracy in time with type A schemes. (a) $\epsilon = 1$. (b) $\epsilon = 10^{-4}$. The reference solution is obtained from the micro-macro for inflow boundaries scheme with $\Delta t = 10^{-4}$.

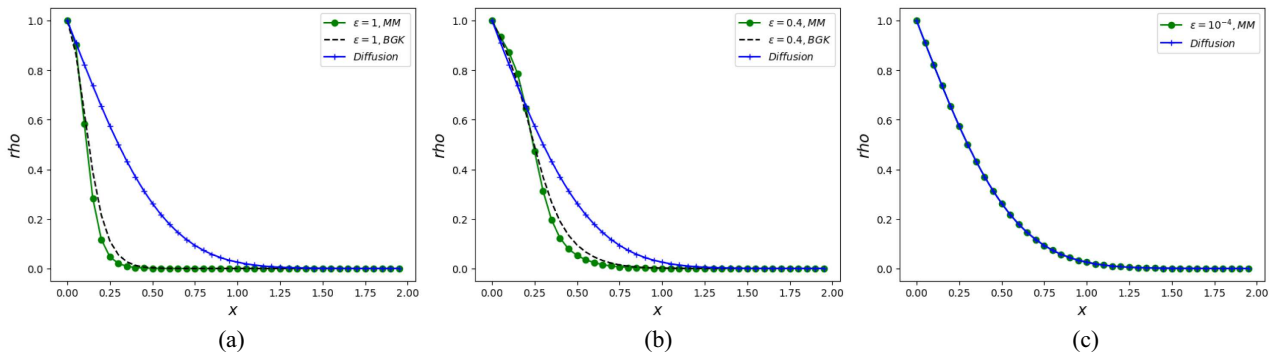


FIGURE 7. Qualitative results for equilibrium inflow at the left boundary. (a) $\epsilon = 1$. (b) $\epsilon = 0.4$. (c) $\epsilon = 10^{-4}$.

order for $\epsilon = 1$ (due to the initial condition). However, for $\epsilon = 10^{-4}$, the required second and third orders respectively are observed.

7.3.2. Qualitative results for equilibrium inflow

In this part, we consider the same problem as before and present a comparison of density plots obtained by using schemes based on micro-macro (MM), full-kinetic (BGK) and diffusion models, for different regimes of ϵ . The boundary conditions for diffusion model $\rho(t, x = 0) = 1$ and $\rho(t, x = 2) = 0$. The final time is $T = 0.1$, $N_x = 40$ and $\Delta t = 0.001$. Further, we consider the same velocity discretization as before for both MM and BGK models. The results for MM are obtained by DP1-A(2, 4, 2) time integrator.

In Figure 7a for rarefied regime ($\epsilon = 1$), the MM and BGK results are in good agreement. In the intermediate regime ($\epsilon = 0.4$) in Figure 7b, the MM and BGK results are still close, and still different from the diffusion one. For $\epsilon = 10^{-4}$, only MM and the diffusion are plotted and are found to be in very good agreement, thereby illustrating the AP property of the numerical scheme for MM.

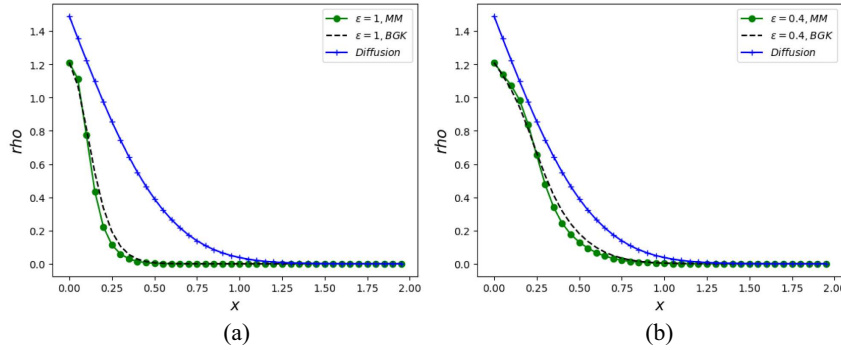


FIGURE 8. Qualitative results for non-equilibrium inflow at the left boundary. $v_{\max} = 5$ and $\Delta v = 1$. $N_x = 40$. (a) $\epsilon = 1$. (b) $\epsilon = 0.4$.

7.3.3. Qualitative results for non-equilibrium inflow

In this part, we consider the same problem as before, but the left boundary condition is chosen as (for $v_k > 0$)

$$f(t, x_i = 0, v_k) = v_k M_k, \quad \bar{\rho}(t, x_i = 0) = \langle f(t, x_i = 0, v_k) \rangle_{V_-} \tag{7.5}$$

$$\bar{g}(t, x_{i+1/2} = -\frac{\Delta x}{2}, v_k) = 2(f(t, x_i = 0, v_k) - \bar{\rho}(t, x_i = 0)M_k) - \bar{g}(t, x_{i+1/2} = \frac{\Delta x}{2}, v_k). \tag{7.6}$$

The final time and time step are the same as in the previous (equilibrium inflow) case. The time integrator used is DP1-A(2, 4, 2). Here, we present a comparison of plots obtained by using schemes based on MM, BGK and diffusion models, for different regimes of ϵ . The scheme described in Section 6.2.1 is used for the micro-macro model and a standard BGK approximation where only inflow boundary condition is needed serves as a reference. For diffusion, the diffusion term is treated implicitly and the left boundary condition for diffusion model is obtained from [23] which translates in our context as:

$$\begin{aligned} \rho(t, x_i = 0) &= \frac{\sum_{v_k > 0} v_k f(t, x_i = 0, v_k) \Delta v}{\sum_{v_k > 0} v_k M_k \Delta v} \\ &+ \frac{1}{\kappa \sum_{v_k} M_k \Delta v} \sum_{v_k > 0} v_k^2 \left(f(t, x_i = 0, v_k) - M_k \frac{\sum_{v_k > 0} v_k f(t, x_i = 0, v_k) \Delta v}{\sum_{v_k > 0} v_k M_k \Delta v} \right) \Delta v. \end{aligned} \tag{7.7}$$

For the continuous in velocity form, the above boundary value is evaluated to be $\rho_0 = \frac{\pi+4}{2\sqrt{2\pi}} \simeq 1.42$.

In Figure 8a for rarefied regime ($\epsilon = 1$), the MM and BGK models compare very well, while the diffusion model is driven by the macro boundary condition. In the intermediate regime ($\epsilon = 0.4$) in Figure 8b, in the MM and BGK results (which are in a good agreement), a boundary layer starts to be created whereas it is not the case for the diffusion model. For $\epsilon = 10^{-4}$, one can see from Figure 9 that MM model develops a boundary layer at the left boundary before aligning with the diffusion model in the interior of the domain. This is consistent with the results observed using first order schemes in literature [8, 23, 29, 30].

Further in Figure 10, we present the numerical results of MM and diffusion models for $\epsilon = 10^{-4}$ with refined velocity grid to demonstrate the difference between boundary values of 1.42 from (7.7) and 1.59 from micro-macro numerical scheme (derived in Sect. 6.2.1).

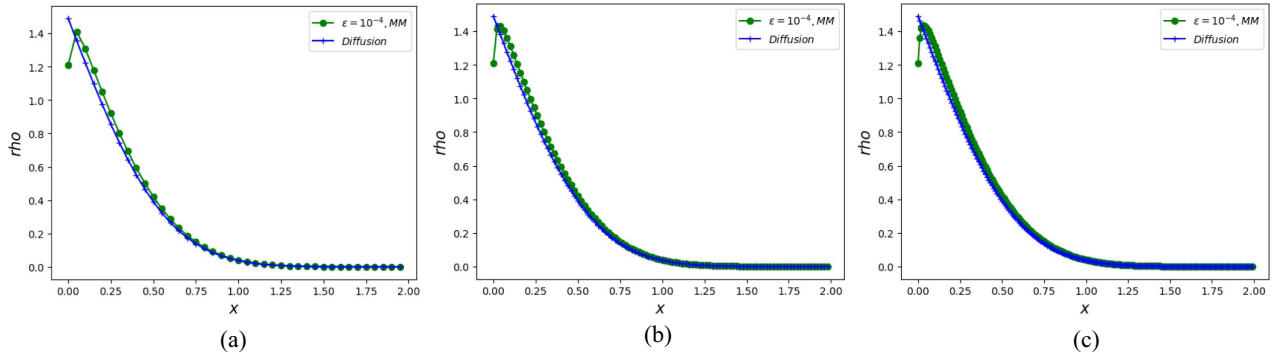


FIGURE 9. Qualitative results for non-equilibrium inflow at the left boundary. $\epsilon = 10^{-4}$. $v_{\max} = 5$ and $\Delta v = 1$ (a) $Nx = 40$. (b) $Nx = 100$. (c) $Nx = 200$.

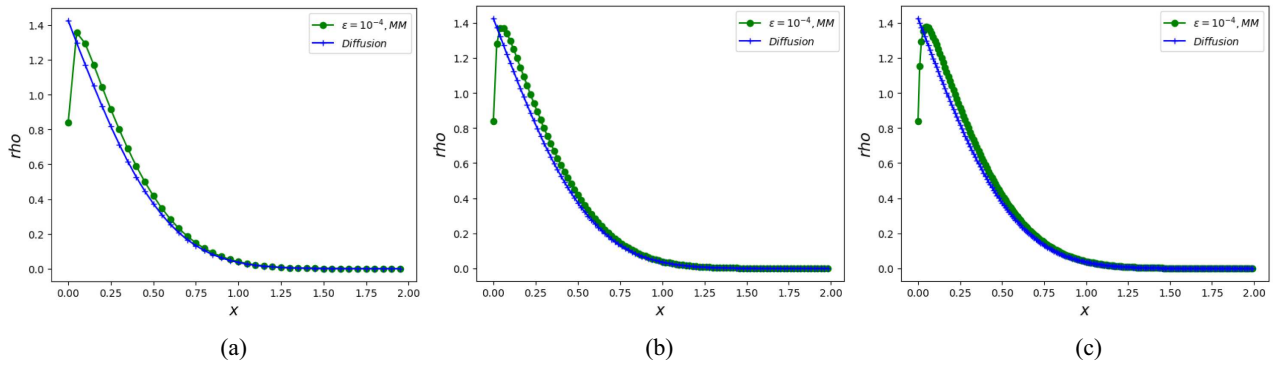


FIGURE 10. Qualitative results for non-equilibrium inflow at the left boundary. $\epsilon = 10^{-4}$. $v_{\max} = 10$ and $\Delta v = 0.125$. (a) $\epsilon = 10^{-4}$, $Nx = 40$. (b) $\epsilon = 10^{-4}$, $Nx = 100$. (c) $\epsilon = 10^{-4}$, $Nx = 200$.

APPENDIX A. MATRIX NOTATION

The circ function is given by:

$$\text{circ}([a_1, a_2, \dots, \underline{a_m}, \dots, a_M]) = \begin{bmatrix} a_m & a_{m+1} & \cdots & a_M & & & a_1 & \cdots & a_{m-1} \\ a_{m-1} & a_m & a_{m+1} & \cdots & a_M & & & \ddots & \vdots \\ \vdots & & & & & \ddots & (0) & & a_1 \\ a_1 & & & & & & & \ddots & \\ & \ddots & & & & & & & \\ & & & & & & & & \\ a_M & & & (0) & \ddots & & & & \\ \vdots & \ddots & & & & & & & \\ a_{m+1} & \cdots & a_M & & & a_1 & \cdots & a_{m-1} & a_m & a_{m+1} \\ & & & & & a_1 & \cdots & a_{m-1} & a_m & a_m \end{bmatrix}. \quad (\text{A.1})$$

The $\text{circ}_b([-1, \underline{1}]_{(N_x-1) \times (N_x-2)})$ function is given by:

$$\text{circ}_b([-1, \underline{1}]_{(N_x-1) \times (N_x-2)}) = \begin{bmatrix} 1 & 0 & \cdots & 0 \\ -1 & 1 & \ddots & \vdots \\ 0 & \ddots & \ddots & 0 \\ \vdots & \ddots & -1 & 1 \\ 0 & \cdots & 0 & -1 \end{bmatrix}_{(N_x-1) \times (N_x-2)}. \tag{A.2}$$

APPENDIX B. BUTCHER TABLEAU

The following is the 2-stage second order accurate Butcher tableau ARS(2, 2, 2):

$$\begin{array}{c|ccc} 0 & 0 & 0 & 0 \\ \gamma & \gamma & 0 & 0 \\ 1 & \delta & 1-\delta & 0 \\ \hline & \delta & 1-\delta & 0 \end{array} \quad \begin{array}{c|ccc} 0 & 0 & 0 & 0 \\ \gamma & 0 & \gamma & 0 \\ 1 & 0 & 1-\gamma & \gamma \\ \hline & 0 & 1-\gamma & \gamma \end{array}.$$

Here, $\gamma = 1 - \frac{1}{\sqrt{2}}$ and $\delta = 1 - \frac{1}{2\gamma}$.

The following is the 4-stage third order accurate Butcher tableau ARS(4, 4, 3):

$$\begin{array}{c|ccccc} 0 & 0 & 0 & 0 & 0 & 0 \\ 1/2 & 1/2 & 0 & 0 & 0 & 0 \\ 2/3 & 11/18 & 1/18 & 0 & 0 & 0 \\ 1/2 & 5/6 & -5/6 & 1/2 & 0 & 0 \\ 1 & 1/4 & 7/4 & 3/4 & -7/4 & 0 \\ \hline & 1/4 & 7/4 & 3/4 & -7/4 & 0 \end{array} \quad \begin{array}{c|ccccc} 0 & 0 & 0 & 0 & 0 & 0 \\ 1/2 & 0 & 1/2 & 0 & 0 & 0 \\ 2/3 & 0 & 1/6 & 1/2 & 0 & 0 \\ 1/2 & 0 & -1/2 & 1/2 & 1/2 & 0 \\ 1 & 0 & 3/2 & -3/2 & 1/2 & 1/2 \\ \hline & 0 & 3/2 & -3/2 & 1/2 & 1/2 \end{array}.$$

For type A, we use 2-stage first order accurate Butcher tableau DP-A(1, 2, 1) ($\gamma \geq \frac{1}{2}$)

$$\begin{array}{c|cc} 0 & 0 & 0 \\ 1 & 1 & 0 \\ \hline & 1 & 0 \end{array} \quad \begin{array}{c|cc} \gamma & \gamma & 0 \\ 1 & 1-\gamma & \gamma \\ \hline & 1-\gamma & \gamma \end{array}.$$

The following is the 4-stage second order accurate Butcher tableau DP2-A(2, 4, 2):

$$\begin{array}{c|cccc} 0 & 0 & 0 & 0 & 0 \\ 0 & 0 & 0 & 0 & 0 \\ 1 & 0 & 1 & 0 & 0 \\ 1 & 0 & 1/2 & 1/2 & 0 \\ \hline & 0 & 1/2 & 1/2 & 0 \end{array} \quad \begin{array}{c|cccc} \gamma & \gamma & 0 & 0 & 0 \\ 0 & -\gamma & \gamma & 0 & 0 \\ 1 & 0 & 1-\gamma & \gamma & 0 \\ 1 & 0 & 1/2 & 1/2-\gamma & \gamma \\ \hline & 0 & 1/2 & 1/2-\gamma & \gamma \end{array}.$$

The following is the 4-stage second order accurate Butcher tableau DP1-A(2, 4, 2) which achieves third order accuracy on the DIRK part:

$$\begin{array}{c|cccc} 0 & 0 & 0 & 0 & 0 \\ 1/3 & 1/3 & 0 & 0 & 0 \\ 1 & 1 & 0 & 0 & 0 \\ 1 & 1/2 & 0 & 1/2 & 0 \\ \hline & 1/2 & 0 & 1/2 & 0 \end{array} \quad \begin{array}{c|cccc} 1/2 & 1/2 & 0 & 0 & 0 \\ 2/3 & 1/6 & 1/2 & 0 & 0 \\ 1/2 & -1/2 & 1/2 & 1/2 & 0 \\ 1 & 3/2 & 1-3/2 & 1/2 & 1/2 \\ \hline & 3/2 & 1-3/2 & 1/2 & 1/2 \end{array}.$$

ACKNOWLEDGEMENTS

Megala Anandan sincerely acknowledges the indispensable support provided by Prof. S. V. Raghurama Rao, whose encouragement was instrumental in the successful completion of this research work.

FUNDING

This work has been partially supported by Centre Henri Lebesgue, program ANR-11-LABX-0020-0.

REFERENCES

- [1] G. Albi, G. Dimarco and L. Pareschi, Implicit-explicit multistep methods for hyperbolic systems with multiscale relaxation. *SIAM J. Sci. Comput.* **42** (2020) 2402–2435.
- [2] U. Ascher, S. Ruuth and R. Spiteri, Implicit-explicit Runge–Kutta methods for time dependent partial differential equations. *Appl. Numer. Math.* **25** (1997) 151–167.
- [3] S. Boscarino and G. Russo, Flux-explicit IMEX Runge–Kutta schemes for hyperbolic to parabolic relaxation problems. *SIAM J. Numer. Anal.* **51** (2013) 163–190.
- [4] S. Boscarino, L. Pareschi and G. Russo, Implicit-explicit Runge–Kutta schemes for hyperbolic systems and kinetic equations in the diffusion limit. *SIAM J. Sci. Comput.* **35** (2013) A22–A51.
- [5] S. Boscarino, L. Pareschi and G. Russo, A unified IMEX Runge–Kutta approach for hyperbolic systems with multiscale relaxation. *SIAM J. Numer. Anal.* **55** (2017) 2085–2109.
- [6] M. Carpenter and C. Kennedy, Additive Runge–Kutta schemes for convection-diffusion-reaction equations. *Appl. Numer. Math.* **44** (2003) 139–181.
- [7] A. Crestetto, N. Crouseilles, G. Dimarco and M. Lemou, Asymptotically complexity diminishing schemes (ACDS) for kinetic equations in the diffusive scaling. *J. Comput. Phys.* **394** (2019) 243–262.
- [8] N. Crouseilles and M. Lemou, An asymptotic preserving scheme based on a micro-macro decomposition for collisional Vlasov equations: diffusion and high-field scaling limits. *Kin. Rel. Models* **4** (2011) 441–477.
- [9] G. Dimarco and L. Pareschi, Exponential Runge–Kutta methods for stiff kinetic equations. *SIAM J. Numer. Anal.* **49** (2011) 2057–2077.
- [10] G. Dimarco and L. Pareschi, Asymptotic preserving implicit-explicit Runge–Kutta methods for nonlinear kinetic equations. *SIAM J. Numer. Anal.* **51** (2013) 1064–1087.
- [11] G. Dimarco and L. Pareschi, Implicit explicit linear multistep methods for stiff kinetic equations. *SIAM J. Numer. Anal.* **55** (2017) 664–690.
- [12] G. Dimarco, L. Pareschi and V. Rispoli, Implicit-explicit Runge–Kutta schemes for the Boltzmann–Poisson system for semiconductors. *Commun. Comput. Phys.* **15** (2014) 1291–1319.
- [13] G. Dimarco, L. Pareschi and G. Samaey, Asymptotic preserving Monte Carlo methods for transport equations in the diffusive limit. *SIAM J. Sci. Comput.* **40** (2018) 504–528.
- [14] Z. Ding, L. Einkemmer and Q. Li, Dynamical low-rank integrator for the linear Boltzmann equation: error analysis in the diffusion limit. *SIAM J. Numer. Anal.* **59** (2021) 2254–2285.
- [15] L. Einkemmer, J. Hu and Y. Wang, An asymptotic-preserving dynamical low-rank method for the multi-scale multi-dimensional linear transport equation. *J. Comput. Phys.* **439** (2021) 110353.
- [16] J. Jang, F. Li, J.-M. Qiu and T. Xiong, Analysis of asymptotic preserving DG-IMEX schemes for linear kinetic transport equations in a diffusive scaling. *SIAM J. Numer. Anal.* **52** (2014) 2048–2072.
- [17] J. Jang, F. Li, J.-M. Qiu and T. Xiong, High order asymptotic preserving DG-IMEX schemes for discrete-velocity kinetic equations in a diffusive scaling. *J. Comput. Phys.* **281** (2015) 199–224.
- [18] S. Jin, Efficient asymptotic-preserving (AP) schemes for some multiscale kinetic equations. *SIAM J. Sci. Comput.* **21** (1999) 441–454.
- [19] S. Jin, Asymptotic preserving (AP) schemes for multiscale kinetic and hyperbolic equations: a review. *Riv. Mat. Univ. Parma* (2012) 177–216.
- [20] S. Jin and D. Levermore, The discrete-ordinate method in diffusive regimes. *Transp. Theory Stat. Phys.* **22** (1993) 739–791.
- [21] S. Jin, L. Pareschi and G. Toscani, Diffusive relaxation schemes for multiscale discrete-velocity kinetic equations. *SIAM J. Numer. Anal.* **35** (1998) 2405–2439.
- [22] S. Jin, L. Pareschi and G. Toscani, Uniformly accurate diffusive relaxation schemes for multiscale transport equations. *SIAM J. Numer. Anal.* **38** (2000) 913–936.
- [23] A. Klar, Asymptotic-induced domain decomposition methods for kinetic and drift diffusion semiconductor equations. *SIAM J. Sci. Comput.* **19** (1998) 2032–2050.
- [24] A. Klar, Asymptotic-induced scheme for nonstationary transport equations in the diffusive limit. *SIAM J. Numer. Anal.* **35** (1998) 1073–1094.

- [25] A. Klar and C. Schmeiser, Numerical passage from radiative heat transfer to nonlinear diffusion models. *Math. Models Methods Appl. Sci.* **11** (2001) 749–767.
- [26] P. Lafitte and G. Samaey, Asymptotic-preserving projective integration schemes for kinetic equations in the diffusion limit. *SIAM J. Sci. Comput.* **34** (2012) 579–602.
- [27] E. Larsen and J. Keller, Asymptotic solution of neutron transport problems for small mean free paths. *J. Math. Phys.* **15** (1974) 75–81.
- [28] M. Lemou, Relaxed micro-macro schemes for kinetic equations. *C. R. Math.* **348** (2010) 455–460.
- [29] M. Lemou and F. Méhats, Micro-macro schemes for kinetic equations including boundary layers. *SIAM J. Sci. Comput.* **34** (2012) B734–B760.
- [30] M. Lemou and L. Mieussens, A new asymptotic preserving scheme based on micro-macro formulation for linear kinetic equations in the diffusion limit. *SIAM J. Sci. Comput.* **31** (2008) 334–368.
- [31] G. Naldi and L. Pareschi, Numerical schemes for kinetic equations in diffusive regimes. *Appl. Math. Lett.* **11** (1998) 29–35.
- [32] L. Pareschi and G. Russo, Implicit-explicit Runge–Kutta methods and applications to hyperbolic systems with relaxation. *J. Sci. Comput.* **25** (2005) 129–155.
- [33] Z. Peng and F. Li, Asymptotic Preserving IMEX-DG-S schemes for linear kinetic transport equations based on Schur complement. *SIAM J. Sci. Comput.* **43** (2021) A1194–A1220.
- [34] Z. Peng, Y. Cheng, J.-M. Qiu and F. Li, Stability-enhanced AP IMEX-LDG schemes for linear kinetic transport equations under a diffusive scaling. *J. Comput. Phys.* **415** (2020) 109485.
- [35] Z. Peng, Y. Cheng, J.-M. Qiu and F. Li, Stability-enhanced AP IMEX1-LDG method: energy-based stability and rigorous AP property. *SIAM J. Numer. Anal.* **59** (2021) 925–954.



Please help to maintain this journal in open access!

This journal is currently published in open access under the Subscribe to Open model (S2O). We are thankful to our subscribers and supporters for making it possible to publish this journal in open access in the current year, free of charge for authors and readers.

Check with your library that it subscribes to the journal, or consider making a personal donation to the S2O programme by contacting subscribers@edpsciences.org.

More information, including a list of supporters and financial transparency reports, is available at <https://edpsciences.org/en/subscribe-to-open-s2o>.